Design & Control of a 1/5th Scaled X-by-Wire Multi-Actuated Research Vehicle (MARV)

Benjamin DeBoer *, Jeremy B. Kimball, Kush Bubbar

Posted Date: 18 March 2026

doi: 10.20944/preprints202603.1426.v1

Keywords: X-by-wire; independent wheel drive and steer; over-actuated vehicle; scaled vehicle; software defined vehicles

 doi:10.20944/preprints202603.1426.v1

Article

Design & Control of a 1/5th Scaled X-by-Wire Multi-Actuated Research Vehicle (MARV)

Benjamin DeBoer *, Jeremy B. Kimball and Kush Bubbar

System-Level Model Development Engineering Lab (Sys-MoDEL), Department of Electrical and Computer Engineering, University of New Brunswick, Fredericton, NB, Canada

* Correspondence: ben.deboer@unb.ca

Abstract

The automotive industry is amidst a shift towards software-defined vehicles (SDV), enabled by the continual integration of X-by-Wire (XBW) technologies into modern vehicle systems. SDVs paired with over-actuated vehicle chassis' enable the potential for a highly optimized vehicle control system by interpreting the driver's actions and directly optimizing the output of one or multiple drive, steer, brake, and suspension-by-wire systems. However, a sim-to-real gap is present between the simulation and full-scale validation of the control systems for over-actuated and SDV systems. This article presents the Multi-Actuated Research Vehicle (MARV), a 1:5 scale over-actuated XBW ground vehicle test platform with independent wheel steer, brake, drive, and suspension-by-wire capability. The scaled MARV platform provides an intermediate step within the sim-to-real gap, enabling a low-risk hardware and software in the loop alternative for advanced control system testing and validation. The MARV platform design is presented as a comprehensive guide for developing a scaled XBW research vehicle, outlining the vehicle's system requirements, engineering specifications, mechanical, electrical, embedded, and control system design. The resulting over-actuated XBW vehicle was constructed and validated against the vehicle's system requirements, creating an intermediate step between simulation and full-scale testing of advanced vehicle control systems in SDVs.

Keywords: X-by-wire; independent wheel drive and steer; over-actuated vehicle; scaled vehicle; software defined vehicles

1. Introduction

As the automotive industry transitions toward software-defined vehicles (SDVs), the ability to algorithmically control key aspects of a vehicle's motion is paramount. To this end, vehicles are increasingly adopting X-by-Wire (XBW) architectures. XBW eliminates mechanical connections between the driver and the vehicle, opting instead for sensors that measure driver input and actuators that respond by controlling the vehicle. A software layer exists between the sensors and actuators to interpret driver intent and command the actuator response based on the current scenario. This new architecture offers substantial benefits over traditional mechanical vehicle control systems, whose performance is heavily constrained by the reaction times and operational skill of humans.

The concept of replacing safety-critical mechanical control linkages with electronic systems is not new. Its origins lie in the aerospace industry, where "fly-by-wire" (FBW) technology revolutionized aircraft design and performance. The commercial turning point in aerospace occurred with the introduction of the Airbus A320 in the late 1980s [1]. Before this, commercial aircraft relied on a complex and heavy network of steel cables, pulleys, and hydraulic lines to transmit pilot inputs to actuators. The A320 introduced a full-authority digital FBW system, where the pilot's inputs were processed by computers and digitally transmitted to the actuators. Previously, a pilot's inputs were direct commands for specific control surfaces; however, with FBW, they are used to determine the pilot's objective, e.g., a request for a specific roll rate or vertical load factor. The computers then

 doi:10.20944/preprints202603.1426.v1

manipulate the actuators to achieve this objective while strictly enforcing flight envelope protections, preventing the aircraft from exceeding its limits regardless of pilot input. These automated protections made possible by FBW drastically improved aircraft safety and realized weight reductions by removing the old mechanical linkages. The automotive industry is undergoing a similar transition. Just as the A320 pilot commands a flight objective, the driver of an X-by-wire vehicle commands a driving objective (e.g,, yaw rate or trajectory), with the on-board systems managing the specific wheel steering angles, drive, and braking torques required to achieve it.

Drive-by-wire (DBW), also known as throttle-by-wire, was one of the first X-by-Wire systems implemented in vehicles. It replaced the mechanical cable between the pedal and the engine with a sensor and microcontroller system. These systems improved fuel economy and emissions by maintaining optimal throttle conditions at all times, and were a critical prerequisite for modern electronic stability control (ESC) systems. DBW was introduced early on because it primarily impacts vehicle performance rather than critical safety, allowing drivers to gain confidence in electronic vehicle systems [2].

Following throttle-by-wire, Brake-by-Wire (BBW) systems evolved from traditional Electro-Hydraulic Brake (EHB) systems to fully Electro-Mechanical Brake (EMB) architectures [3,4]. EHB serves as a transitional technology by replacing the vacuum booster with an electric motor or high-pressure accumulator while retaining hydraulic actuation. EMB is further advanced by eliminating the hydraulic system in favor of motors mounted directly at the wheels. Both of these systems enable independent wheel braking, faster response times, and seamless integration with regenerative braking systems.

Similarly, Steer-by-Wire (SBW) eliminates the mechanical steering column with a purely electrical connection, enabling variable steering ratios and active stabilization interventions [5,6]. This decoupling improves handling performance and ultimately safety, but requires force feedback actuators to artificially recreate road feel to maintain a satisfying driving experience.

Concurrently integrating these three X-by-Wire subsystems via holistic control methods maximizes the potential of SDVs, and is an active area of research. For example, coordinating SBW with differential braking (BBW) or driving forces (DBW) at individual wheels allows the vehicle to maintain stability in extreme maneuvers where traditional mechanical systems would fail [7]. Like any safety-critical control system, these X-by-Wire systems require comprehensive hardware validation. Due to the relatively recent emergence of this paradigm, there is little openly disseminated knowledge of X-by-Wire test platforms. An example is the Stanford X1 [8], a student-designed steer-by-wire and drive-by-wire research vehicle, that utilizes independent rear electric drive and high-fidelity GPS/INS to validate control strategies near tire saturation limits. Similarly, the Toyota Research Institute (TRI) GRIP platform [9] serves as a robust testbed via 'dynamics emulation', utilizing all-wheel steering (AWS), four-wheel independent drive (4WID), and four-wheel independent braking (4WIB) to replicate the behavior of various vehicle configurations. A four-wheel independent steer (4WIS), 4WID, and 4WIB testbed is the KTH Research Concept Vehicle [10]. This platform also includes active camber control, offering even more flexibility in terms of evaluating the vehicle behaviour and extending the type of advanced control strategies that can be implemented. RoboMObil (ROMO) from the German Aerospace Center (DLR) is an X-by-Wire test platform which takes a modular approach, consisting of four identical wheel robots, each consisting of electronically controllable drive motors, brakes, steering, and dampers [11]. These powerful vehicle dynamics control test platforms are extremely important for final algorithm validation on hardware, but are prohibitively expensive for smaller research groups to build. Therefore, many promising vehicle dynamics control strategies remain untested on physical hardware.

Testing and validating control and estimation algorithms on full-scale hardware can be dangerous and costly, and simulation is still not sufficiently advanced for complete validation of safety-critical software. Scaled test platforms offer a compromise between these two extremes. They enable algorithm testing in a low-risk development environment, while still forcing consideration of practical hardware implementation, such as compute constraints, measurement fidelity, and actuation dynamics. To

 doi:10.20944/preprints202603.1426.v1

contextualize the design of a scaled X-by-wire testbed, it is necessary to examine the existing landscape of scaled vehicle test platforms.

One of the most common scaled vehicle testbeds is the RoboRacer (F1TENTH) platform [12]. Designed as a community benchmark for autonomous racing, it utilizes a standard 1:10 scale TRAXXAS RC car platform with a single drive motor and steering servo, and adds a LIDAR and cameras. Several other autonomy-focused scaled testbeds exist, such as the 1:10 scale RACECAR platform from MIT [13], the 1:10 scale Berkeley Autonomous Race Car (BARC) from the University of California Berkeley [13], and the 1:5 scale AutoRally platform from Georgia Institute of Technology [14]. Although these vehicle designs have been extremely successful in increasing the accessibility of autonomous driving research, their simplified mechanical architecture limits their utility for the validation and testing of advanced vehicle dynamics control methods for XBW vehicles.

One scaled test platform that offers some of the over-actuation necessary for X-by-Wire research is the Nigel platform [15]. This vehicle includes independent all-wheel driving and independent all-wheel steering. However, the Nigel platform is 1:14 scale, where low mass, small tires, and lack of a suspension can lead to erratic dynamics that are not necessarily representative of a full-scale vehicle.

This article presents the Multi-Actuated Research Vehicle (MARV), a 1:5 scale XBW ground vehicle test platform with independent wheel: i) SBW, ii) BBW, iii) DBW, and iv) suspension-by-wire (active suspension) capability. The MARV platform fills the gap between simulation and full-scale XBW vehicle validation, enabling a low-risk alternative for advanced control system testing and validation. The article presents the design of the MARV platform as a comprehensive guide for developing a scaled XBW research vehicle.

The platform design is presented as follows: First, Section 2 provides an overview of the motivation and requirements for the vehicle, outlining system requirements and engineering specifications. Section 3 outlines the vehicle's mechanical design, followed by the electrical, embedded, and low-level control system design in Section 4. The full vehicle assembly is presented in Section 5, following by system identification and experimental validation of key vehicle requirements in Sections 6 and 7. Finally, Section 8 concludes and presents avenues of future work.

2. System Requirements & Engineering Specifications

To ensure the MARV platform, depicted in Figure 1, effectively bridges the gap between simulation and full-scale validation, its development was guided by a top-down design methodology. The platform's core objective is to be vehicle-agnostic, with the capability to represent a wide range of full-scale vehicles by configuring the vehicle's software, or at most, minimizing the number of affected subsystems. To achieve this level of versatility, a list of the high-level system requirements was established, which in turn dictates the engineering specifications for each of the platform's core subsystems.

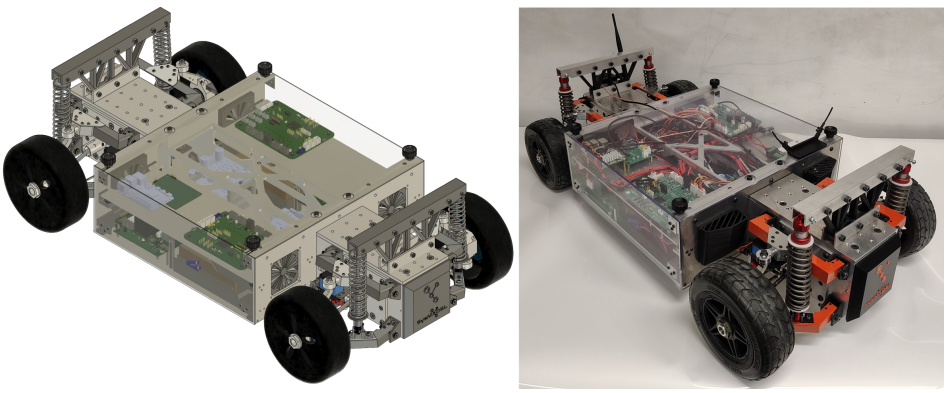

Figure 1. Left: Two axle MARV platform design. Right: Manufactured and tested MARV platform.

 doi:10.20944/preprints202603.1426.v1

2.1. System Requirements

The MARV platform must meet several high-level performance and functional requirements to serve as an effective tool for advanced vehicle dynamics and control research. These vehicle system requirements (VSRs) are identified as:

- **VSR1: X-by-Wire Architecture:** The platform must use a complete XBW architecture with independent corner control, including DBW (independent wheel torque), SBW (independent wheel steering), BBW (independent wheel braking torque), and suspension-by-wire (independent corner suspension force).
- **VSR2: Full State Feedback:** The system must provide full state feedback for the 18-DOF vehicle for use in advanced control algorithms. The DOFs include 6-DOF for the chassis, 4-DOF for each driveline, 4-DOF for each steering system, and 4-DOF for each suspension.
- **VSR3: Dynamic Performance:** The platform must meet 1/5th scaled performance targets that are representative of a broad range of full-scale vehicles.
    a. **Acceleration:** 0 to 5.26 m/s (a scaled 0-60 mph) in $<$ 5.2 seconds.
    b. **Top Speed:** A top speed of 16.67 m/s (60 km/h).
    c. **Braking:** A 5.26 m/s to 0 scaled stopping distance of $<$ 7.68 meters.
    d. **Wheel Spacing:** Wheel spacing 0.66 m long, 0.4 m wide
    e. **Turning Radius**: A scaled turning radius of $<$ 2.30 m.
- **VSR4: Modularity and Adjustability:** Key vehicle parameters must be adjustable to replicate the dynamics of various vehicles. This includes modular drive, braking, steering, and suspension components.
- **VSR5: Remote Operation and Monitoring:** The platform must be capable of full remote control, real-time monitoring, and data logging of control inputs and all system states.
- **VSR6: High-Level Control Interface:** The system must provide a well-defined Application Programming Interface (API) to facilitate the implementation and testing of vehicle control algorithms.

2.2. Engineering Specifications and Subsystem Design

To meet the system-level requirements, the vehicle's design is discretized into the core subsystems of: 1) Chassis, 2) Driveline, 3) Suspension, 4) Steering, 5) Braking, and 6) Embedded System designs. Due to the extensive number of engineering requirements needed to achieve an effective system design, only key requirements for each subsystem are presented below and referenced throughout the article.

2.2.1. Chassis

The chassis design directly affects system-level requirements VSR3 and VSR4; specifically, its core role is to facilitate the wheel spacing of VSR3 and modularity and adjustability requirements of VSR4. A critical design decision is the selection of a body-on-frame design over a unibody construction. While unibody designs offer advantages in weight and rigidity for mass-manufactured passenger cars, a simple body-on-frame approach is better suited for a scaled research testbed for several reasons:

- **Modularity:** The separation of the frame from the body allows for easy modification and access to components.
- **Strength:** For a scaled vehicle, a rigid frame is ideal as it provides sufficient strength in a simple package.
- **Repairability:** In the event of damage, repairing or replacing components of a body-on-frame design is simpler than repairing a complex, integrated unibody structure.
- **Manufacturability:** A body-on-frame is significantly easier to manufacture using simple manufacturing mills and lathes, as opposed to the required sheet metal forming and welding of a unibody design.

 doi:10.20944/preprints202603.1426.v1

The body-on-frame selection results in both frame and body specifications. The frame engineering specifications (FES) are:

- **FES1:** The vehicle frame shall provide a uniform mounting interface at each axle location, allowing the vehicle to be adapted to any suspension, driveline, braking, and steering subsystem configurations.
- **FES2:** The frame shall provide structural mounting points for the vehicle body and include pathways for power distribution, sensor cabling, and system communication.
- **FES3:** The frame must bear the static and dynamic vehicle loads due to the vehicle's mass and projected dynamic loads.
- **FES4:** The frame's top surface shall incorporate a standardized mounting grid to accommodate vehicle hardware and provide expansion capacity for extra sensors.
- **FES5:** The frame's bottom surface shall incorporate a standardized mounting grid to facilitate cable management and attachment of internal subsystem hardware.

The body interacts directly with the vehicle frame, with the body engineering specifications (BES) of:

- **BES1:** The body shall provide dedicated housing and mounting points for the battery pack, power distribution modules, embedded systems, and control modules.
- **BES2:** The body shall be removable from the frame as a single assembly.
- **BES3:** The body must incorporate a thermal management system to ensure the body's internal operating temperature remains below the specified limits of the BES1 components.

2.2.2. Driveline

The vehicle is specified to have independent wheel drive-by-wire (DBW) defined by VSR1, facilitated by electric drive motors. The DBW requirements stem from VSR3, specifically the acceleration and top speed requirements. The driveline engineering specifications (DES) are defined as:

- **DES1:** The driveline must achieve the desired torque and velocity profiles to achieve VSR3-a and VSR3-b, in front or rear drive operation modes.
- **DES2:** The driveline must interface with the standardized mounting points in FES1.

2.2.3. Braking

Dynamic requirement VSR3-c directly informs the need for an independent brake-by-wire system. The brake-by-wire engineering specification (BrES) is:

- **BrES1:** The braking system must stop the vehicle within a distance of 7.68 m from an initial velocity of 5.26 m/s (VSR3-c), using either the front or rear braking systems.

2.2.4. Suspension

The role of the vehicle suspension system is to elevate the chassis from the road and isolate the vehicle from road disturbances. The following key suspension engineering specifications (SES) are:

- **SES1:** The suspension must maintain a static ground clearance of 50 mm at the 1G (loaded) design ride height.
- **SES2:** The suspension systems with steering must exhibit a positive mechanical trail to generate wheel self-aligning torque.
- **SES3:** The suspension shall be designed to minimize the wheel's scrub radius.
- **SES4:** The suspension shall exhibit negative camber during suspension compression and positive camber during extension.
- **SES5:** The suspension's mounting points on the vehicle frame must align with FES1
- **SES6:** The suspension must have a natural frequency between $1 - 2$ Hz, with a damping ratio of $0.2 - 0.4$ [16].
- **SES7:** The suspension must incorporate a mounting interface for an active suspension actuator to apply force directly on the unsprung mass.

 doi:10.20944/preprints202603.1426.v1

2.2.5. Steering

The steer-by-wire system will be designed as a four-wheel independent steering system. The steering engineering specifications (STES) are defined as:

- **STES1:** The steering system must apply an effective steering angle for each wheel compensating for bump steer throught suspension travel.
- **STES2:** The steering system must achieve a two-wheel, either front or rear axle steering turning radius defined in VSR3-d.

2.2.6. Embedded & Compute Systems

The vehicles' embedded systems and onboard main compute module (MCM) have four core responsibilities, defined as embedded engineering specifications (EES):

- **EES1:** The embedded system must monitor the vehicle's power supply and ensure safe charge and discharge.
- **EES2:** The embedded system must regulate and safely distribute the power supply voltage to the vehicle's subsystems.
- **EES3:** The embedded control architecture must implement low-level actuator control and sensing to achieve the desired wheel effective steering angle, drive motor, and braking torque, and active suspension force.
- **EES4:** The MCM must implement remote monitoring, real-time data logging, and sub-module communication, specified by VSR5 and VSR6.

The presented requirements and specifications establish the framework for the MARV architecture. To achieve the necessary performance within these constraints, a highly integrated mechatronic design approach was adopted. The following sections detail the realization of this design, presenting the mechanical, electrical, and embedded systems design for each subsystem of the XBW platform. To provide a concise overview, these sections outline the implemented design, backed by the fundamental system analysis.

3. Mechanical Design

The core guiding principle of the mechanical design process was to maximize modularity and adjustability (VSR4) in each subsystem design. This led to the adoption of various off-the-shelf 1/5th scale vehicle components, specifically ball joints, wheels, tires, tie-rods, suspension struts, and driveshafts. The mechanical design targets robustness and incorporates design for manufacturing considerations. Throughout early iterations of the design, it became clear that the $1/5^{\text{th}}$ scale XBW vehicle can be designed within a maximum vehicle mass of 35 kg, encompassing the full mechanical design, batteries, and electrical components. Therefore, throughout the analysis of the vehicle's systems design, an estimated vehicle mass of $m_v = 35$ kg will be used. The following five sub-sections detail the mechanical design of the chassis, driveline, braking, suspension, and steering subsystems to address the engineering specifications presented in Sections 2.2.1 to 2.2.5.

3.1. Chassis Design

The selected body-on-frame chassis design is distributed into independent frame and body designs to fulfill the FES and BES specifications. The body and frame interact directly through FES2, incorporating standard mounting points on the frame and body for ease of assembly.

3.1.1. Frame Design

The frame design facilitates the placement and structure required to mount the chassis' body and each of the vehicle's mechanical subsystems. The objective is to create a frame design that can be easily adapted for an increase in vehicle wheelbase. The vehicle specifications outline a wheelbase aspect ratio of 1.65 (VSR3 - 0.66 m wheelbase, 0.4 m track width), which represents a shorter vehicle. By designing the vehicle at the 1.65 wheelbase aspect ratio (VSR3), the frame experiences it's tightest

 doi:10.20944/preprints202603.1426.v1

spatial constraint; where larger aspect ratio vehicles can be realized by simply increasing the distance between the two axles.

Analyzing the engineering specifications FES1 and FES2 and their location on a traditional vehicle, the frame design was separated into two portions: the axle portion (FES1) and the body portion (FES2), see Figure 2. Inspired by the box frame design within mass-produced pickup trucks, the frame is designed from a single 4.5" x 4.5" extruded square tube of 6063 Aluminum, 3/16" thick. Aluminum was selected as the core frame material due to its high strength-to-weight ratio and extrusion properties. The strength-to-weight ratio allows the frame to withstand worst-case scenario impact forces (FES3) while remaining sufficiently light to aid in the vehicle's dynamic performance criteria (VSR3).

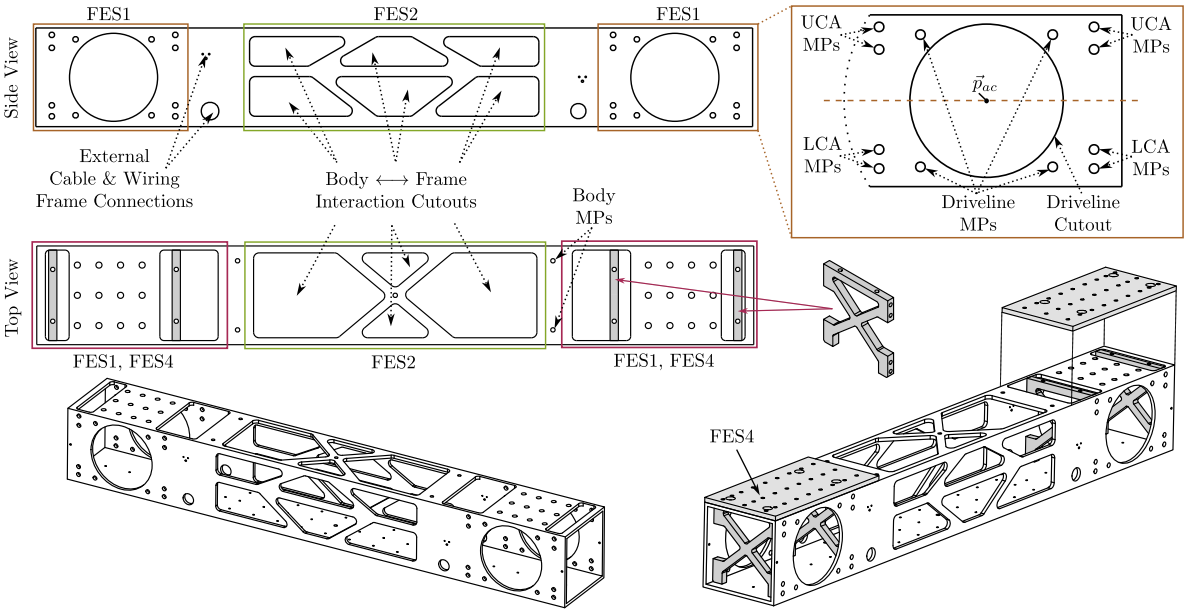

Figure 2. Chassis frame design, identifying the critical areas relating to FES1, FES2, and FES4. The figure highlights the mounting points (MPs) for the upper (UCA) and lower control arm (LCA), body, and driveline, displaying the frame's modular design (VSR4).

The frame design, depicted in Figure 2, has three main topologies: the side profile (mirror front to back and side to side), the top, and the bottom. The side profile is responsible for fulfilling FES1 and FES2. To address FES1, a generic motor mounting location and suspension mounting locations are defined in reference to the axle's center point (see $\vec{p}_{ac}$ in Figure 2). The $\vec{p}_{ac}$ is selected based on a 170 mm diameter 1/5th scale tire (Rovan RV89002), where a distance > 85 mm from the edge of the frame ensures the wheel is longitudinally contained within the footprint of the vehicle frame. The body design, discussed below, has a maximum length of 400 mm, bounding the geometry of FES2. The objective of FES2 is to maximize the interaction space between the body and frame, facilitated by a large cutouts within the frame's tube.

The FES1 and FES2 requirements also extend to the frame's top, creating access points for installing and mounting the axle's subsystems and facilitating the wiring of the vehicle. These access points are covered by a standardized mounting grid for vehicle hardware and sensors (FES4). To facilitate both access to the axle's subsystems and employing a standardized mounting point for the vehicle's strut and future exteroceptive sensors, 3 components were added to the frame design for each axle. The first 2 components are structural cross members placed between the left and right control arm mounting points. The cross members extend to the top of the vehicle's frame, facilitating a strong mounting point connection for the 3rd component, a 1/4" thick aluminum top plate. The top plate allows for extreme adaptability, harnessing equidistantly placed holes to mount vehicle hardware and exteroceptive sensors (such as lidar or stereo cameras). An application example of FES4 is the supporting structure for the vehicle's strut, which requires a mounting point significantly higher than the presented frame mounting points (MP) in Figure 2.

 doi:10.20944/preprints202603.1426.v1

The frame's bottom topology is equipped with equidistant threaded holes throughout the frame for FES5, facilitating the mounting of hardware and cable management within the frame at the discretion of the selected axle design.

3.1.2. Body Design

The vehicle's body is responsible for housing the batteries, electronics, and computing hardware (BES1). In full-scale EVs, the batteries are integrated into the base of the vehicle chassis and/or frame, leading to a lower center of gravity. This method was directly implemented within the MARV design; the body was separated into upper and lower levels. The lower level contained the batteries and required power electronics and battery monitoring systems. The upper level is dedicated to the mounting of embedded systems and compute modules, described in Section 4. A key difference in a scaled vehicle is that the batteries are generally removed from the vehicle to be recharged. This difference led to the development of a drawer system within the body, where the body's lower level can slide out from under the upper level, allowing direct access to the batteries for removal and recharging.

The core objective of the body's design is to enable easy mounting and removal from the vehicle's frame (BES2). Therefore, the body's structure was designed to sit directly on top of the frame (see body mounting points in Figure 2), with the bulk of the body wrapping around the sides of the frame. The body is primarily designed from aluminum, with vibration dampeners placed between the body's main structure and the upper and lower body plates. Stock 6" drawer slides are employed to facilitate the motion of the lower tray assembly, with ball detents and screw knobs used to hold the tray closed during operation. The top, bottom, and sides of the body are made from 1/8" clear polycarbonate sheet, allowing the vehicle's operator to visually inspect the batteries, embedded systems, and compute modules without opening the body.

To cool the electronic systems within the body (BES3), four 80 mm computer fans with an airflow rating of 18.9 ft^3/min are placed at the front and rear of the body to provide airflow over the batteries and electrical components. The total volume of the body is 2.35e−2 m^3 (0.829 ft^3). With all four fans operational (two input fans, two exhaust fans), the air within the body is cycled 45 times per minute. Additional blower fans are added throughout the vehicle body to ensure adequate passive cooling for all electronic devices. Figure 3 displays the body design, highlighting the body's layer structure, mounting method, and main cooling fan locations.

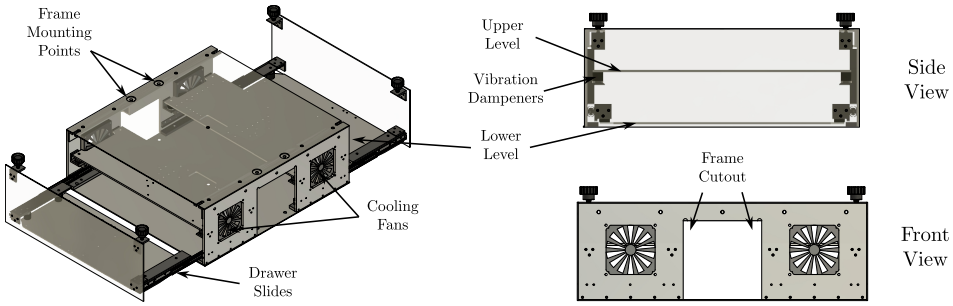

Figure 3. Chassis body design - incorporating a sliding lower tray and fixed upper tray with cooling fans mounted at the body's front and rear.

3.2. Driveline Design

The vehicle's driveline is responsible for providing the independent wheel propulsive power required to obtain the maximum speed and acceleration rate defined in VSR3. An electric vehicle's powertrain can be separated into the driveline (motors and gearboxes) and the power supply (batteries). The core trade-off when selecting the driveline motor is the comprise between the motor's power and its geometry and weight.

The drive motor selection is constrained by the vehicle's top speed (60 km/h - VSR3-b) and acceleration requirements (0 $\rightarrow$ 5.36 m/s in 5.3 s - VSR3-a). Assuming the motor can apply a constant

 doi:10.20944/preprints202603.1426.v1

torque throughout the acceleration, the required longitudinal chassis force to meet the acceleration requirement, neglecting aerodynamic drag and mechanical losses, is defined as:

$$F_a = ma = (35\text{ kg})\left(\frac{5.36\text{ m/s}}{5.3\text{ s}}\right) = 35.39\text{ N}. \tag{1}$$

To achieve the acceleration requirement with only the front or rear drivelines enabled (DES1), the peak motor torque (τ_p) for each driveline must be:

$$\tau_p = \frac{1}{2}F_a r_t = 1.50\text{ Nm}, \tag{2}$$

where $r_t = 85$ mm is the tire's radius, neglecting tire deflection. Similarly, the peak vehicle speed (VSR3-b of 60 km/h) informs the peak driveline velocity (ω_p) defined as:

$$\omega_p = \frac{v_s}{r_t} = 196.08\text{ Rad/s}. \tag{3}$$

Due to the high torque requirement, a large-diameter motor was selected, eliminating the need for an integrated gearbox. This decision minimizes the overall length and weight of the driveline assembly, ensuring it remains within the vehicle frame design. The CubeMars RI Series Brushless Direct Current (BLDC) frameless motor line was identified as candidate drive motors. The RI80 (85 mm diameter) and RI100 (104 mm diameter) motors exceeded τ_p, with a motor peak torque of 4.28 Nm (19.42 A) and 4.98 Nm (23.33 A), respectively. Additionally, the motors met the required peak motor speeds of 196.08 rad/s with supply voltages of 24.96 V and 17.83 V.

The second core component of the vehicle's powertrain is a portable power source capable of providing high current to the drive motors. Lithium polymer (LiPo) batteries were selected as the candidate power supply for their compact size, high current output, and wide adoption in scaled vehicles. Each LiPo cell has a voltage ranging from 3.2 V (discharged) to 4.2V (charged) with 3.7 V considered the average LiPo voltage for analysis. Since mass-produced LiPo batteries are limited to 6 cells (22.2 V). Multiple battery packs must be wired in series to achieve the supply voltage > 25 V, leading to the selection of 8-cell (two 4-cell batteries) and 9-cell (three 3-cell batteries) battery configurations for further analysis. These configurations provide nominal power supply voltages of 29.6 V and 33.3 V, respectively.

To select the best powertrain combination, lumped parameter acceleration and top speed simulations were conducted for both motors in Matlab's Simscape toolbox. The simulation considers the motor's electrical and mechanical characteristics to accelerate the vehicle while considering air resistance and rolling resistance. The simulation is conducted with two drive motors enabled. The air resistance parameters were set to conservative values, with a drag coefficient of $C_d = 0.40$, a frontal area of $A_d = 0.12\text{ m}^2$, and an air density of $\rho = 1.20\text{ kg/m}^3$. The results of the lumped parameter simulations are displayed in Figure 4. The RI80 and RI100 motors are both capable of achieving the maximum speed and acceleration requirements with one of the supply voltages. Ultimately, the RI80 motor with a nominal supply voltage of 33.3 V was selected, due to its smaller diameter and reduced maximum current, compared to the KI100. The reduced diameter decreases the motor's footprint in the vehicle frame, while the reduced peak current allows for smaller wire gauge and power electronics to be implemented. The result is a vehicle capable of achieving a $0 \rightarrow 5.36$ m/s acceleration in 1.97 s, while reaching the desired top speed within 7.89 s.

The driveline design is displayed in Figure 5, targeting 3 main objectives: 1) Implement a motor casing and rotor to interface with the KI80 frameless motor, 2) deliver the motor's torque to the driveshaft, and 3) create mounting points for the future steer-by-wire motors. The frameless BLDC motor allows the designer to create custom motor shaft/rotor and stator mounting designs. The motor shaft was designed with a 8 mm output shaft and a press fit interaction with the BLDC's rotor. The stator housing was designed based on the motor cutout diameter in FES1 of Figure2 aligning with

 doi:10.20944/preprints202603.1426.v1

DES2, with the BLDC stator press fit into the stator housing. The motor's back plate was designed with the same outer radius as the stator housing, covering the stator and supporting a bearing. The motor's front plate is responsible for mounting the driveline assembly to the frame, using the specified bolt pattern in FES1, providing attachment points for the future steering system, and houses a bearing for the motor's output shaft. The assembly is held together by counter-sunk flat-head six screws, passing through the countersunk front plate and stator housing and threading into the back plate, creating a clamping force between the front and rear motor plates while ensuring alignment of the motor's stator and rotor.

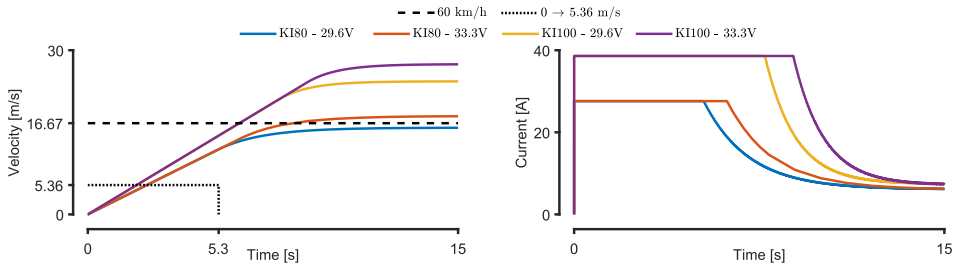

Figure 4. Reduced order simulation results displaying the vehicle velocity (left) and drive motor current (right) response to step inputs of 29.6 V and 33.3 V. The dashed line represents the desired maximum vehicle speed, and the dotted line represents the desired acceleration characteristics.

The proposed driveline design achieves the vehicle acceleration (VSR3-a) and top speed (VSR3-b) requirements. The electric powertrain requirement also influences the required vehicle stopping distance (VSR3-c), covered in the following section.

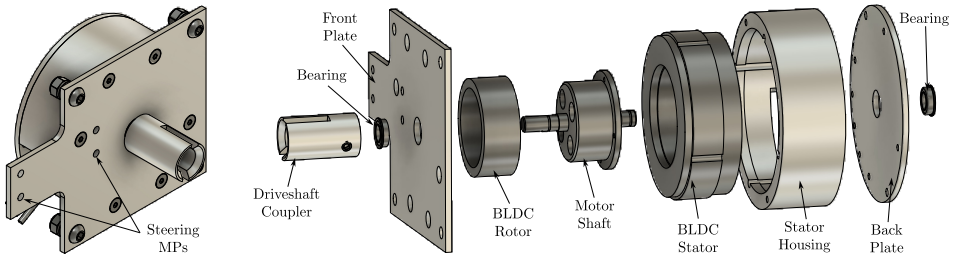

Figure 5. Driveline mechanical design, comprised of a custom front plate, rear plate, stator housing, motor shaft, and coupler. designed to incorporate the frameless BLDC motor. The driveline front plate incorporates standard mounting points (MPs) for the steering subsystem.

3.3. Brake System Design

The vehicle's braking system is responsible for rapidly and accurately dissipating the vehicle's kinetic energy. With EVs, a significant amount of the energy can be transferred back into the batteries, provided the batteries can accept the charge. However, when the batteries are fully charged, the EV relies on dissipative braking capabilities, such as resistor banks and traditional mechanical braking systems. The required energy dissipation by the braking system (E_b) to stop a vehicle can be defined by:

$$E_b = \frac{1}{2}mv^2 = l_b F_b \tag{4}$$

where l_b is the desired braking distance, and F_b is the required braking force applied to the chassis. Using (4) in the context of BrES1, a constant dissipative force of $F_b = 65.47$ N is required to achieve the $l_b = 7.68$ m stopping distance. With equal brake force engagement on either the front or rear wheels, the required braking torque for each wheel as:

$$\tau_b = \frac{r_t F_b}{2} = 2.78 \text{ Nm}. \tag{5}$$

 doi:10.20944/preprints202603.1426.v1

The peak torque the RI80 motor can achieve is 4.28 Nm, showing that regenerative braking alone is sufficient in achieving the required stopping distance. However, a traditional mechanical braking system is required in two scenarios: First, if the vehicle's battery is full regenerated braking can not be used. Second, the mechanical brakes act independently of the motors, allowing increased energy dissipation in emergencies.

In a previous work, the authors developed a mathematical model for a cable-based disk-brake system [17]. The $1/5^{\text{th}}$ scale system, which consists of a cable-based brake caliper, is modified to be adopted for the designed vehicle. Based on the determined coefficient of friction $\mu_{pr} = 0.443$ between the aluminum brake pad and carbon fiber rotor in [17], the applied braking force by the caliper must be:

$$F_{pr} = \frac{\tau_b}{r_r \mu_{pr}} = 187.33 \text{ N} \tag{6}$$

to stop the vehicle within 6.78 m, where $r_r = 33.5$ mm is the radius between the wheel center and the centroid of the brake pad and rotor contact surface. The clamping force is within the tested and verified range of 25 N to 250 N of the system presented in [17].

In this application, the scaled brake caliper was modified by replacing the lever arm that drives the caliper with a disk of fixed diameter (30 mm). In doing so, the mechanical advantage of the caliper assembly is reduced to 5 : 1, resulting in a peak cable force of 37.47 N. The required cable stroke can be determined by referencing the 90° operational range of the calipers' internal cam system (see Figure 6), leading to a maximum stroke of 23.6 mm. Due to the limited cable displacement and force requirements, a servo motor was selected to drive the system. A driven spool with a diameter of 11 mm was mounted to the servo, resulting in a peak motor torque of 0.41 Nm and an angular displacement of 245°. The torque is within the operation range of 25 and 35 kg-cm (2.45 and 3.43 Nm) servo motors. Figure 6 displays the design of the braking system, connecting the servo motor and driving spool located in the vehicle frame with the 1/5th scale caliper and drive disk on the wheel hub.

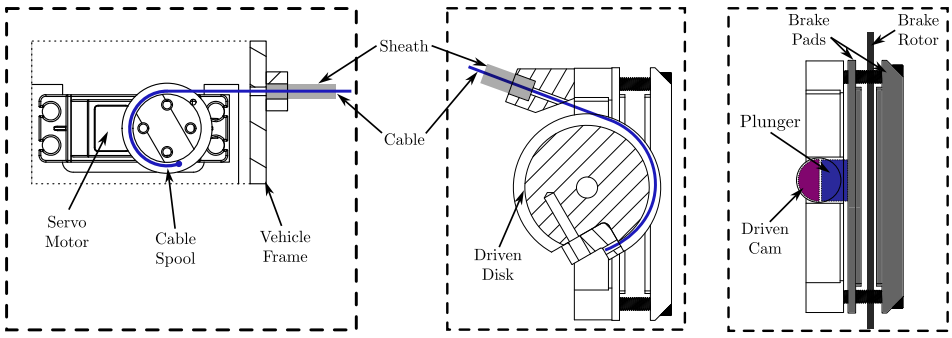

Figure 6. Brake-by-wire system diagram, depicting the chassis-mounted actuator (left), knuckle-mounted caliper (center), and the interworking of the cam-based brake caliper (right). The chassis-mounted actuator drives the cable spool creating tension on the cable, where the cable is connected to the driven disk on the caliper through a cable sheath. The driven disk rotates the driven cam in caliper (right) pushing the plunger and inner brake pad towards to brake rotor.

3.4. Suspension Design

The suspension system elevates and isolates the vehicle from road disturbances, all while maintaining consistent tire contact with the road. In analyzing steerable suspension designs, both the McPherson Strut and Double-wishbone suspensions allow for tailoring of the suspension's behaviour by changing the positions of key kinematic points (referred to as hardpoints) in the suspension (i.e. ball joints, wheel bearings). Ultimately, the double wishbone suspension was selected for both the front and rear axles of the MARV design due to its high degree of tunability. To aid future applications of both McPherson Strut and Double-wishbone MARV suspension designs, the analysis required to achieve the vehicle's 1-G ground clearance, suspension stiffness and damping, and universal mounting requirements (SES1 - SES3) are presented.

 doi:10.20944/preprints202603.1426.v1

Before starting the suspension design, it is important to create a local reference frame for the axle's suspension system. The local frame is placed on the bottom of the vehicle's frame (Z), aligning with the axle's center point ($\vec{p}_{ac}$). Unless otherwise specified, all suspension hardpoints and designs are expressed relative to this local frame. This concept of suspension hardpoints and local suspension frames was inspired by the Project Chrono Vehicle open source library [18]. The relevant hardpoints to fully define the Double-wishbone and McPherson strut suspension designs are illustrated in Figure 7.

The suspension design begins by specifying the position of the wheel hub ($\vec{p}_{hub}$), the point where the wheel is mounted to the suspensions knuckle. Its position is fully defined by the 1-G ground clearance $h_{gc} = 50$ mm (SES1), vehicle wheel-base and track-width, and knowledge of the wheel and tire specifications. The selected 1/5th scale vehicle wheel and tire boasts an outer radius (r_{out}) of 85 mm, a tread width of 60 mm, an inner rim radius (r_{in}) of 61.5 mm, and a hub offset (w_{off}) of +21.88 mm. Assuming negligible tire deformation, the Z component of the wheel hub ($\vec{p}_{hub}$) can be defined by the tire radius, ground clearance, and camber, where the X and Y component are defined by the wheelbase and track width, respectively. The local suspension reference frame positions the assembly longitudinally (accounting for the wheelbase), while the Y component is determined by referencing the wheel offset, desired track width (l_{tw}), and camber. The result is a fully defined wheel hub position of

$$\vec{p}_{hub} = \begin{bmatrix} 0 \\ \frac{l_{tw}}{2} + \Big(w_{off}\cos(\beta_{1G}) + r_{out}\sin(\beta_{1G})\Big) \\ \Big(r_{out}\cos(\beta_{1G}) + w_{off}\sin(\beta_{1G})\Big) - h_{gc} \end{bmatrix} \tag{7}$$

for the left side vehicle suspension, where β_{1G} is the desired tire camber angle at the 1-G position. Due to the inherent symmetry between the left and right suspension designs, the identified hardpoints for the vehicle's left side are reflected to the right by flipping the sign of the Y component. The second hardpoint defined is the position of the wheel bearing ($\vec{p}_{brg}$) determined by:

$$\vec{p}_{brg} = \vec{p}_{hub} - l_{spl}\begin{bmatrix} 0 \\ \cos(\beta_{des}) \\ -\sin(\beta_{des}) \end{bmatrix} \tag{8}$$

where l_{spl} is the spindle length, defined as the distance between the wheel hub and the end of the wheel bearing. This length incorporates the vehicle's disk braking system and axle bearing systems. The alignment of the $\vec{p}_{brg}$ and $\vec{p}_{hub}$ X components ensures the wheel has zero steering angle. With the initial wheel and tire position defined, the focus can shift to achieving the desired suspension characteristics outlined in SES2 to SES4.

The McPherson Strut and Double-wishbone suspensions both implement a lower control arm (LCA), connecting the vehicle frame with the knuckle assembly with a revolute joint and ball joint. To ensure sufficient design space for the wheel bearing and knuckle geometry, the Z component lower ball joint position ($\vec{p}_{lbj}$) is constrained based on the wheels inner diameter, such that the Z component between $\vec{p}_{lbj}$ and $\vec{p}_{brg}$ is $> \frac{1}{2}r_{in}$. The ball joints X and Y components informs the vehicle's mechanical trail (SES2), scrub radius (SES3), and camber (SES4). These specifications are dependent on the suspension's kingpin axis ($\hat{k}$ - a unit vector), and its change throughout suspension compression and extension. In the McPherson strut design, $\hat{k}$ is defined between $\vec{p}_{lbj}$ and the upper strut mount ($\vec{p}_{usm}$) located on the chassis, see Figure 7, as:

$$\hat{k} = \frac{\vec{p}_{usm} - \vec{p}_{lbj}}{\|\vec{p}_{usm} - \vec{p}_{lbj}\|}. \tag{9}$$

 doi:10.20944/preprints202603.1426.v1

Where, in the double-wishbone design, $\hat{k}$ is defined between $\vec{p}_{lbj}$ and the upper ball joint ($\vec{p}_{ubj}$) as:

$$\hat{k} = \frac{\vec{p}_{ubj} - \vec{p}_{lbj}}{\|\vec{p}_{ubj} - \vec{p}_{lbj}\|}. \tag{10}$$

The kingpin axis directly enables calculation of the mechanical trail and scrub radius. A simplified calculation of the mechanical trail (l_{mech}) and scrub radius (l_{scrub}) is defined as:

$$\begin{bmatrix} l_{mech} \\ l_{scrub} \end{bmatrix} = \begin{bmatrix} \hat{x} \\ \hat{y} \end{bmatrix} \cdot \left(\left(\vec{p}_{lbj} - \hat{k} \cdot \frac{\left(r_{out}\cos(\beta) + w_{off}\sin(\beta) \right)}{\hat{k}_z} \right) - \vec{p}_{tp} \right), \tag{11}$$

with

$$\vec{p}_{tp} = \vec{p}_{hub} - \begin{bmatrix} 0 \\ \left(w_{off}\cos(\beta) + w_{Rad}\sin(\beta) \right) \\ \left(w_{Rad}\cos(\beta) + w_{off}\sin(\beta) \right) \end{bmatrix} \tag{12}$$

where $\vec{p}_{tp}$ is the center location of the tire print. The wheel camber (β) can be determined by the change in the Y component of $\hat{k}$ due to the suspension's motion, defined as:

$$\beta_l = \arcsin\left(\hat{y} \cdot \left(\hat{k} - \hat{k}_{1G} \right) \right) + \beta_{1G} \tag{13}$$

for the vehicle's left side, where $\hat{k}_{1G}$ is $\hat{k}$ at the suspensions 1G position. These simplified calculations in (11) - (13) are only valid in zero-steer conditions.

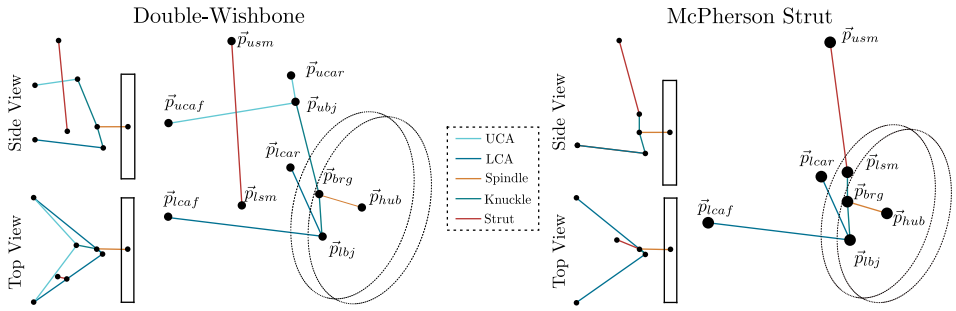

Figure 7. Left: Double-Wishbone suspension hardpoints. Right: McPherson Strut suspension hardpoints.

The SES2 - SES4 suspension requirements outline a positive mechanical trail, near-zero scrub radius, while achieving negative camber during suspension compression and positive camber during suspension extension. Analyzing the camber characteristics in (13) and the definition of $\hat{k}$ in (10) outlines that to have negative camber during compression, the Y component of $\vec{p}_{lbj}$ must increase while the Y component of the $\vec{p}_{ubj}$ decreases (double-wishbone) or remains constant (McPherson). The opposite is required to generate positive camber during suspension extension. Simply put, the Z component of $\vec{p}_{lbj}$ must be less than the LCA mounting points ($\vec{p}_{lca}$) on the frame, creating a 1-G LCA angle $\theta_{LCA-1G} < 0°$. As the suspension is compressed ($\theta_{LCA} > \theta_{LCA-1G}$), the Y component of $\vec{p}_{lbj}$ increases, resulting in negative camber. Therefore, for bounded LCA rotation of $\theta_{LCA} \in [0°, -90°]$, the camber is inversely proportional to the θ_{LCA} deviation from the 1-G position. To amplify the camber characteristics from the LCA, the double-wishbone's UCA can incorporate a similar design methodology, but instead apply a positive 1-G UCA angle ($\theta_{LCA-1G} > 0°$).

The LCA and UCA frame mounting points are defined based on the frame's axle interface layout (FES1), outlined in SES4. For simplicity, the front and rear LCA ($\vec{p}_{lcaf}$ and $\vec{p}_{lcar}$) and UCA ($\vec{p}_{ucaf}$ and $\vec{p}_{ucar}$) mounting points are placed with identical Y components, leading to the UCA and LCA rotating about the vehicle's X axis.

 doi:10.20944/preprints202603.1426.v1

To achieve the characteristics in SES2-SES5, systematic iteration of the suspension hardpoints for the specified suspension type (see Figure 7) is applied. The resultant hardpoints for left side double wishbone suspension designs implemented in the MARV platform are expressed in Table 1. The suspension design boasts a mechanical trail of 14.39 mm, scrub radius of 0.52 mm, and camber range of 3.81° to −6.93° for LCA rotations of −20.0° (extension) and 21.2° (compression) from θ_{LCA-1G}.

Table 1. Suspension design hardpoints for the left front and rear suspension systems.

		$\vec{p}_{ubj}$	$\vec{p}_{ucaf}$	$\vec{p}_{ucar}$	$\vec{p}_{lbj}$	$\vec{p}_{lcaf}$	$\vec{p}_{lcar}$	$\vec{p}_{hub}$	$\vec{p}_{brg}$	$\vec{p}_{usm}$	$\vec{p}_{lsm}$
Front	x	−8.22	84.20	−84.20	5.94	84.20	−84.20	−2.06	−1.04	43.32	46.41
	y	142.00	72.55	72.55	184.01	72.55	72.55	174.07	224.26	111.06	125.31
	z	111.61	101.60	101.60	−0.64	12.70	12.70	33.88	33.98	174.61	26.52
Rear	x	−8.22	84.20	−84.20	6.42	84.20	−84.20	−1.85	−3.19	−42.68	−37.12
	y	142.01	72.55	72.55	184.01	72.55	72.55	173.91	224.09	111.06	129.94
	z	111.56	101.60	101.60	−0.64	12.70	12.70	33.99	33.81	174.94	25.86

With the suspension's core positional characteristics achieved, focus can shift to the suspension's response to road disturbances, defined by SES6. The suspension's stiffness and damping are facilitated by the strut. The strut acts as a variable-length link with connection points on the vehicle frame ($\vec{p}_{usm}$) and LCA (double-wishbone) or knuckle (McPherson Strut). In suspension design, the goal is to keep the suspension's natural frequency between 1 and 2 Hz, with lower natural frequencies leading to increased ride comfort and higher natural frequencies for increased dynamic performance [19]. To determine the required stiffness and damping of the combination strut, a 1-DOF linear quarter-car suspension model is referenced, with transfer function:

$$\frac{Z_s(s)}{Z_r(s)} = \frac{b_{QC}s + k_{QC}}{\frac{m_v}{4}s^2 + b_{QC}s + k_{QC}}. \tag{14}$$

where Z_s and Z_r are the vertical positions of the sprung mass and road, respectively, and k_{QC} and b_{QC} are the suspension's stiffness and damping. The natural frequency of the second-order linear system is determined by:

$$\omega_n = \sqrt{\frac{4k_{QC}}{m_v}}, \tag{15}$$

leading to a desired quarter-car stiffness of:

$$k_{QC} = \frac{1}{4}m_v\omega_n^2. \tag{16}$$

Analyzing the stiffness for both comfort (1 Hz) and performance (2 Hz) natural frequencies yields quarter-car stiffnesses of 345 N/m and 1382 N/m, respectively. In the same way the suspension's damping coefficient is determined by:

$$b_{QC} = \frac{1}{2}m_v\zeta\omega_n. \tag{17}$$

Applying damping ratios of 0.2 (comfort) - 0.4 (performance) (values from Table 3 of [16]), leads to damping coefficients of 138 Ns/m and 1105 Ns/m for comfort and performance designs, respectively.

The quarter car suspension model is built on the assumption that the spring and damper are placed directly above the tire contact point. Therefore, scaling is required to determine the stiffness (k_{st}) and damping (b_{st}) of the physical strut from the quarter car parameters. The coefficients are scaled based on the strut's unit vector ($\hat{h}$) and its connection to the unsprung mass - upright for the McPherson strut and LCA for the double-wishbone. The coefficients are determined as:

 doi:10.20944/preprints202603.1426.v1

$$\begin{bmatrix} k_{st} \\ b_{st} \end{bmatrix} = \begin{bmatrix} k_{QC} \\ b_{QC} \end{bmatrix} \left(\frac{{}^{C}\vec{p}_{tp-y} - {}^{C}\vec{p}_{lca-y}}{\left({}^{C}\vec{p}_{lsm-y} - {}^{C}\vec{p}_{lca-y}\right) \cdot {}^{C}\hat{h}_{-z}} \right)^2 \tag{18}$$

where C denotes the chassis frame with $-y$ and $-z$ extracting the vectors Y and Z component, and ${}^{C}\hat{h}$ is defined as:

$${}^{C}\hat{h} = \frac{{}^{C}\vec{p}_{usm} - {}^{C}\vec{p}_{lsm}}{\|{}^{C}\vec{p}_{usm} - {}^{C}\vec{p}_{lsm}\|}. \tag{19}$$

An important metric when selecting or designing the strut's spring is the required pre-load to suspend the vehicles at its 1-G position. The pre-load can be determined by referencing the required spring displacement at 1-G, as:

$$\Delta_{st-1G} = \frac{\frac{1}{4} m_v g \left({}^{C}\vec{p}_{tp-y} - {}^{C}\vec{p}_{lca-y}\right)}{k_{st} {}^{C}\hat{h}_{-z} \left({}^{C}\vec{p}_{lsm-y} - {}^{C}\vec{p}_{lca-y}\right)}. \tag{20}$$

The presented suspension design analysis covers kinematic and dynamic requirements of a passive suspension system outlined in SES1 - SES6. The final engineering specification outlines implementation of an independent wheel active suspension (SES7).

3.4.1. Active Suspension

The MARV archecture was designed to enable the future integration of a fully active suspension system. The suspension-by-wire system, including the actuator and linkage, have not been fully defined. Based on past active suspensions for scaled vehicles, it is assumed that active suspension system will be electrically driven by a direct current (DC) motor. To properly scale the vehicles power distribution and battery capacity for a future active suspension system a quarter-car simulation was conducted to establish power baselines.

A 2-DOF quarter-car simulation was conducted, implementing comfort-oriented quarter-car parameters: $m_s = 7.0$ kg, $m_u = 1.75$ kg, $k_s = 345$ N/m, $c_s = 138$ Ns/m, and $k_t = 40$ kN, representing the sprung mass, unsprung mass, suspension stiffness and damping, and tire stiffness, respectively. A Linear Quadratic Regulator (LQR) was designed to optimize the suspension's ride comfort at a constant speed of 40 km/h over an ISO 8608 Class D road profile, representing a rough/damaged surface [20]. Under these conditions, the simulation yielded a peak mechanical power requirement of 214.98 W, with an average of 18.68 W. Therefore, the electrical subsystem will be specified to include headroom for a peak electrical power requirement of 300 W per wheel for active suspension to account for efficiency and thermal losses.

3.4.2. Suspension CAD

The design of the suspension geometry was the result of iterative design, incorporating standard off-the-shelf 1/5th scale vehicle components. Suspension components in modern vehicles are toplogically optimized; however, for the simplicity of manufacturing, the design focused on creating simple and robust components, capable of being manufactured on a standard 3-axis milling machine and 2-axis lathe. The designed suspension hardpoints are displayed in Table 1 for both the left front and rear suspension designs. Two stock 1/5th scale components were utilized in the design: a combination strut with a removable spring (Rovan RC RV95145), and stock ball joints (Rovan RC RV95108). The lower and upper control arms and corresponding control arm mounts are manufactured from stock mild steel angle iron and tube, respectively. The bulk of the remaining components are manufactured from 6061 Aluminum due to their larger footprint and low mechanical load. To measure the current position of the suspension, an absolute encoder is mounted to the LCA, directly measuring θ_{LCA}. The CAD model of the left front suspension design is presented in Figure 8, resulting in an estimated quarter car mass of 1.34 kg.

 doi:10.20944/preprints202603.1426.v1

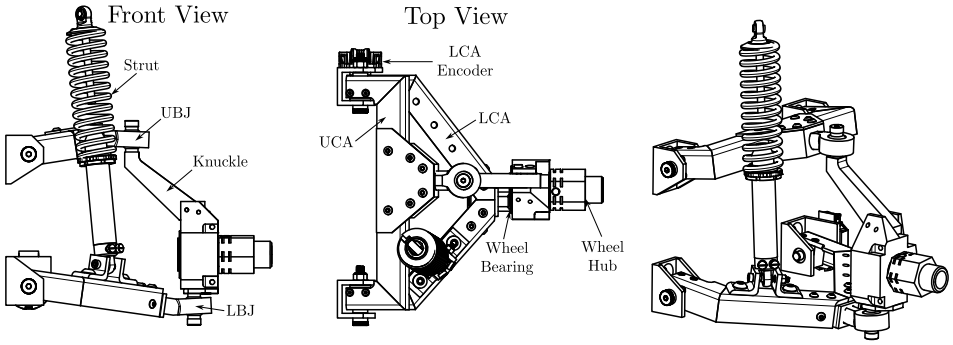

Figure 8. Front left suspension design, displaying the key components and hardpoints.

3.5. Steering System Design

The goal of a traditional linked vehicle steering system is to steer the left and right wheels according to the Ackermann steering condition, resulting in a yaw moment and a lateral force being applied to the vehicle. In SBW systems, the objective shifts to applying an effective steering angle for each wheel, where traditional steering conditions such as Ackermann steering can be applied electronically by the control system designer.

The effective steering angle can be defined by analyzing the x component of the spindle unit vector ($\hat{s}$), defined as:

$$\hat{s} = \frac{\vec{p}_{hub} - \vec{p}_{brg}}{\|\vec{p}_{hub} - \vec{p}_{brg}\|} \tag{21}$$

where the effective steering angle is determined by:

$$\delta_{eff} = \arcsin(-\hat{s}_x) \tag{22}$$

for the vehicle's left side. The sign is flipped for the vehicle's right side, ensuring that the wheels are referencing rotation about the positive Z axis.

To implemented SBW within the suspension design and achieve an effective steering angle, three steering hardpoints and one actuation vector must be defined: the tie-rod connection to the knuckle ($\vec{p}_{trk}$), the tie-rod connection to the steering motor linkage ($\vec{p}_{trm}$), the initial position of the rotational (i.e. pitman arm) or translation (i.e. rack & pinion) steering motor ($\vec{p}_{sm}$) and the motor's rotational or translational unit vector ($\hat{m}$), see Figure 9. In traditional linked steering systems, the linkage is designed to minimize the effects of bump steer, a phenomenon where a compression or extension of the suspension results in a change in the effective steering angle. Bump steer can be minimized by designing the tie-rod hardpoints to align with the UCA and LCA rotational instantaneous center (IC). However, the IC is dynamic with the compression and extension of the suspension; therefore, the design of traditional steering linkages becomes complex. SBW combined with XBW significantly simplifies the steering system design, as with knowledge of the suspension position, the XBW steering actuator can actively compensate for bump steer irrespective of steering hardpoint placement.

For the presented suspension design, an independent wheel pitman arm steering system was applied. The rotational design was selected for it's mechanical simplicity over the rack and pinion design. To implement the pitman arm design, a servo motor was chosen due to its compact size, gearing, and integrated position control. The fidelity of the SBW positional accuracy and feedback is dependent on the mechanical advantage (MA) of the steering linkage, where a simplified mechanical advantage is defined as:

$$MA = \frac{l_{st-m}}{l_{st-k}}, \tag{23}$$

where l_{st-m} is the length of the rotational arm on the motor motor's rotation frame (M) and l_{st-k} is the distance between the tie-rod mount on the knuckle and the $\hat{k}$ axis, in the king-pin frame (K), defined as:

 doi:10.20944/preprints202603.1426.v1

$$l_{st-m} = \left|\left| R_M^C(\vec{p}_{trm} - \vec{p}_{sm}) \right|\right|_{XY} \tag{24}$$

$$l_{st-k} = \left|\left| R_K^C\left(\vec{p}_{trk} - \vec{p}_{lbj}\right) \right|\right|_{XY} \tag{25}$$

where R_M^C and R_K^C denote the rotation matrices to project the points from the chassis frame (C) onto the M and K frames, aligning the $\hat{m}$ and $\hat{k}$ vectors to the frames' $+Z$ axis. Therefore, the XY norm ($\|\cdot\|_{XY}$) represents the effective lever arm for each rotational system.

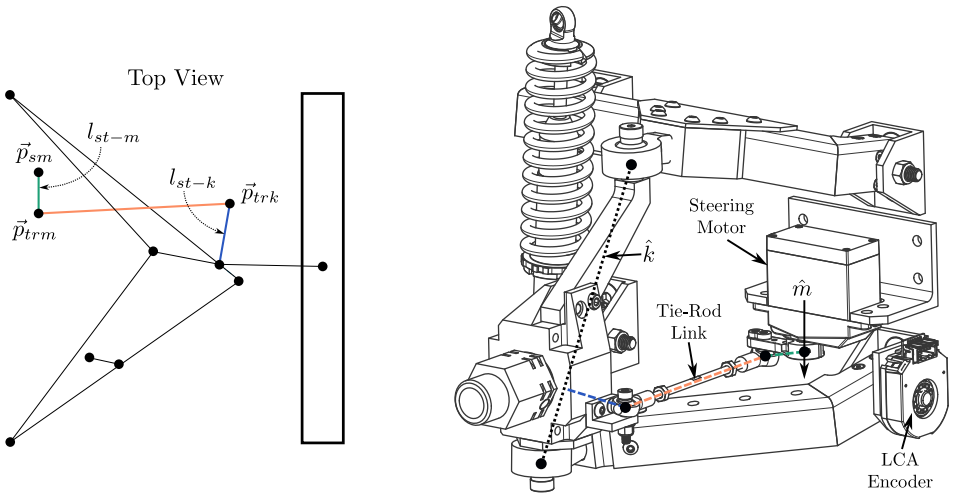

Figure 9. Left: Steering system design hardpoints. Right: Implement steering system CAD design, outlining the tie-rod link, steering motor, and kingpin axis ($\hat{k}$).

A small mechanical advantage (< 1) increases the steering system accuracy and reduces the peak torque required by the steering motor. However, two considerations need to be considered: First, the full effective steering angle range must be achieved. Second, as mechanical advantage increases, the precision of the steering torque feedback is reduced. Steering torque applied onto the kingpin axis can be inferred by measuring the applied torque from the steering motor and calculating the mechanical advantage based on the current suspension and steering link positions. Since the main objective of the XBW steering system is to accurately apply effective steering angles (STES1) a lower mechanical advantage is preferred.

The mechanical advantage limit is based on the desired vehicle turning radius of 2.3 m defined in STES2 and VSR3-e, informing the maximum required effective steering angle to achieve the turning radius. Using the Ackerman steering principle of an IC, the maximum effective front or rear wheel steering angle to achieve a turning radius (r_{tr}) is determined by:

$$\delta_{eff-tr} = \arctan\left(\frac{l_{wb}}{r_{tr} - l_{tw}/2}\right) \tag{26}$$

where the above equation assumes the vehicle's center of mass is at the center of the vehicle's wheelbase. Using the platforms wheel base ($l_{wb} = 0.66$ m) and track width ($l_{tw} = 0.4$ m), a turning radius of 2.30 m leads to a maximum effective steering angle of $\delta_{eff-tr} = 17.4°$.

Taking the design criteria into account, an iterative mechanical design process was conducted, analyzing the location of the selected hardpoints with the desired steering characteristics and mechanical interference. The selected hardpoints and actuation vectors for the left front and rear steering geometries are presented in Table 2. Simulating the combined suspension and steering systems, Figure 10a displays the resultant wheel camber, mechanical trail, and jacking distance for the front left wheel for an effective steering angle range of $\delta_{eff} \in [-0.5, 0.5]$ Rad. The figure clearly demonstrates that the suspension design has significant mechanical trail for the majority of effective steering angles (SES2)

 doi:10.20944/preprints202603.1426.v1

and has a consistently low scrub radius (SES3). The jacking distance is a key metric to consider for independent wheel drive systems, as a suspension with a non-zero caster angle will generate steering (jacking) torque based on the vertical tire load. In traditional linked steering systems, the magnitude of the jacking torque is significantly reduced by the mirrored suspension geometry and is not generally considered. Figure 10b, displays the required steering motor actuation to achieve the effective steering angle at the 1G position and Figure 10c displays the required motor actuation to maintain zero effective steering angle throughout suspension compression and extension.

Table 2. Steering hardpoints for the left front & rear steering systems.

		$\vec{p}_{trm}$	$\vec{p}_{trk}$	$\vec{p}_{sm}$	$\hat{m}$			$\vec{p}_{trm}$	$\vec{p}_{trk}$	$\vec{p}_{sm}$	$\hat{m}$
	x	−26.75	−31.55	−46.75	0		x	31.75	32.69	46.75	0
Front	y	86.33	179.19	86.33	0	Rear	y	86.33	179.30	86.33	0
	z	22.58	24.10	29.68	−1		z	22.58	24.53	29.68	−1

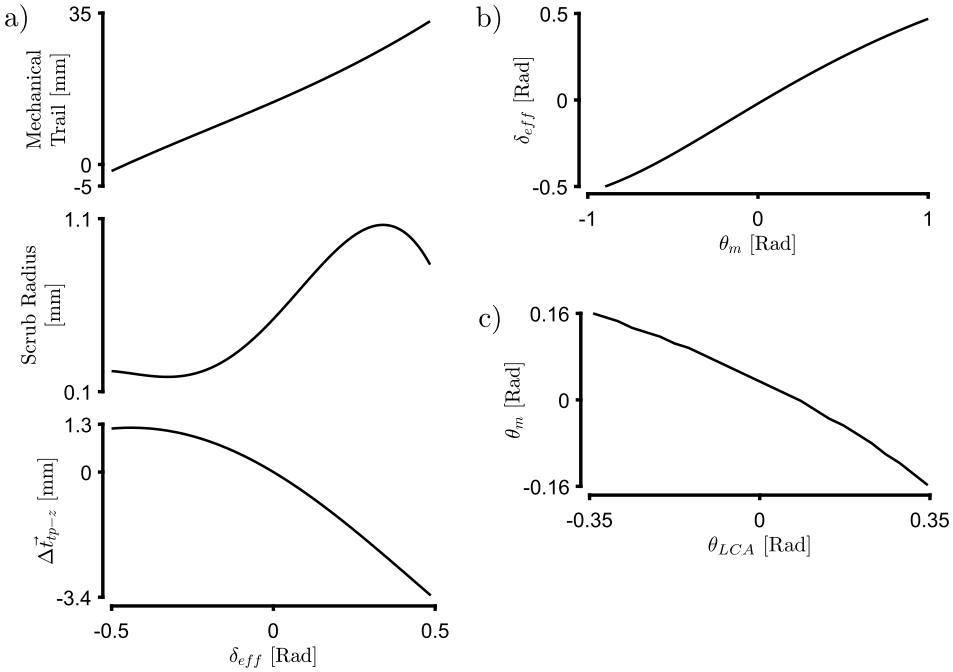

Figure 10. Front left suspension characteristics. a) Presents the mechanical trial, scrub radius, and jacking distance in the tire frame, b) displays the tire's effective steering angle (δ_{eff}) based on the position of the steering motor, and c) outlines the required position of the steering motor to account for bump steer throughout suspension compression and extension.

The steering system mechanical design is presented in Figure 9. The steering motor mount and knuckle tie-rod mount are manufactured from stock 1/8" steel angle with the mounting holes aligning with the drive motor design and knuckle design, respectively. The tie-rod is made from standard 3mm ball joint rod ends and threaded rod, with the distance between the two rod ends defined by the length

$$l_{tr} = ||\vec{p}_{trm} - \vec{p}_{trk}||. \tag{27}$$

The presented mechanical design and analysis initializes the XBW vehicle architecture (VSR1), implementing the mechanisms and systems required to enable independent wheel drive, steer, brake, and suspension-by-wire capabilities. Additionally, the vehicle's dynamic performance (VSR3) and modularity (VSR4) are achieved in the mechanical design and analysis. However, the vehicle's functional efficacy is only realized with integration of an advanced electrical and embedded system architecture to monitor and control the vehicle and its subsystems.

 doi:10.20944/preprints202603.1426.v1

4. Electrical & Embedded System Design

The role of the vehicle's electrical and embedded system design is to bring the mechanical systems to life. Upon analysis of the VSRs and EES', five main objectives for the electrical and embedded system were outlined: 1) Monitor the vehicle's power supply and ensure safe charge and discharge, 2) Facilitate safe distribution and regulation of the power supply voltage to the vehicles subsystems, actuators, sensors, and logic boards, 3) Enable low-level actuator control and sensing for each of the vehicle's subsystems for SR1 and SR2, 4) Achieve requirements VSR1, VSR5 and VSR6 by implementing actuator commands, receive vehicle feedback, enable remote monitoring, real-time data logging, and sub-module communication, and 5) Create an isolated capability to stop vehicle operation in the case of emergencies.

The objectives led to the development of three embedded systems to address the first three objectives, a system-on-module to facilitate objective 4), and a custom wireless emergency stop (E-stop) system to enable 5). Figure 11, displays the vehicle's embedded system architecture, separating the architecture into the axle and chassis levels.

The axle level contains the first three embedded systems, centralized in the vehicle's axle or axle group. Each axle is equipped with an embedded control system (ECS) responsible for controlling the axles actuators and measuring feedback from each axle subsystem. The ECS and corresponding actuators and sensors are energized by a power pack capable of powering one or more axles based on the design specifications. Each power pack contains the LiPo batteries (BAT), a Cell Management System (CMS), and a Power Distribution System (PDS).

The chassis-level contains two independent systems, the main compute module (MCM) and an E-stop module. The MCM is responsible for achieving objective 4), directly interfacing with each axle's ECS on the axle level to command actuator outputs and receive feedback measurements. The MCM is also responsible to provide remote monitoring data to the vehicle's operator, as depicted in Figure 11. In turn, the vehicle's operator is equipped with an E-stop controller intended to safely and rapidly de-energize the vehicle upon activation. The E-stop controller wirelessly communicates with the chassis level E-stop module. The E-stop module interfaces with the PDS module of each power pack, with the capacity to directly disconnect power to the vehicle's energy-inducing actuators.

The segmentation of the system architecture into a chassis and axle level subsystems enables direct scalability for future multi-axle (> 2) vehicles without modifying the core embedded systems (VSR4). A high-level overview of the axle and chassis-level systems is described in the following sub-sections.

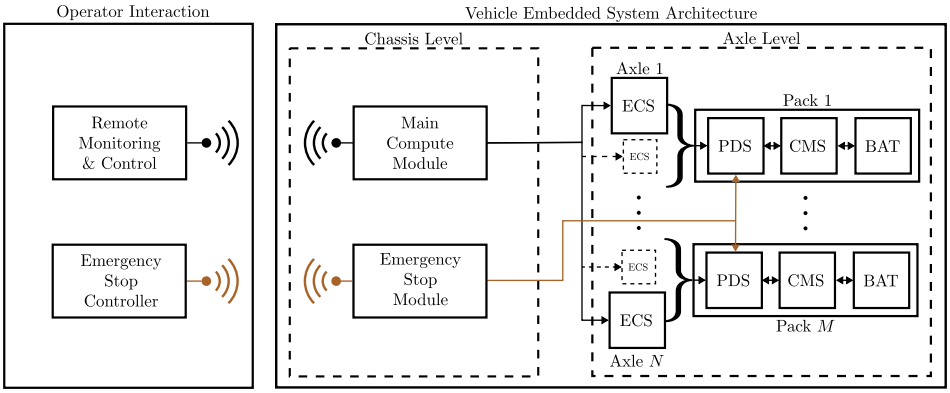

Figure 11. MARV embedded system architecture, separated into chassis and axle level systems. The axle level harnesses the ECS' and power packs required to energize and control the actuators, sensors, and embedded systems. The chassis level coordinates the actuation and obtains feedback from each axle with the MCM. The E-stop module has the capability to directly de-energize the axle level actuators. The operator interacts with the vehicle by monitoring the MCM module over a wireless connection and operating the E-stop controller.

 doi:10.20944/preprints202603.1426.v1

4.1. Axle Level

The core objective of the axle-level system architecture is to achieve the desired control output and provide the required state-feedback measurements for each subsystem in the axle. The power pack's role is to provide the necessary voltage regulation and power supply to the actuators, sensors, and compute systems. The ECS's role is to accurately control the actuators and measure the axle's current state. Each of the power pack embedded systems and the axle ECS are described as follows.

4.1.1. CMS

The CMS is responsible for the monitoring and management of the vehicle's batteries. In Section 3.2, LiPo batteries were selected as the power source for the vehicle, due to the high power/current to weight ratio. LiPo batteries impose a significant safety hazard if improperly charged or discharged. Therefore, the sole objective of the CMS is to ensure the safe operation of the LiPo batteries.

Research into industry available battery and cell management systems led to selecting the TIDA-00449 Texas Instruments reference design [21], capable of managing the discharge and charge of up to a 10 cell LiPo battery packs. Within the design, the core BQ76930 battery management system (BMS) integrated circuit (IC) provides individual cell voltage monitoring, short and overcurrent protection, and an integrated coulomb counter. The reference design was directly integrated with the battery protection circuitry modified according to the combined peak current draw of the powered actuators. The CMS ensures safe power dissipation and energy storage from the equipped LiPo batteries. The managed power supply is then passed through a fused connection to the PDS module for voltage regulation and distribution.

4.1.2. PDS

The vehicle's electrical and embedded systems require a variety of supply voltages for the sensors, actuators, microcontrollers, and compute units. The PDS has two main objectives: 1) Regulate the input voltage from the CMS (33.3 V) to power the internal cooling fans (12.0 V), servo actuators (7.4 V), and sensors and microcontrollers (5 V and 3.3 V), 2) Safely disconnect power to the energy-inducing actuators (the drive motors and active suspension actuators) during emergency stop conditions.

To generate the regulated voltage from the provided CMS voltage, current-mode control buck converters were designed using the WEBENCH Power Designer Tool by Texas Instruments, achieving the first objective. The second objective outlines an essential capability of any experimental platform, the ability to directly disconnect power from the actuators that apply propulsive power to the system, in this case, the main drive motors and future active suspension motors. Therefore, the power for these systems is routed through the PDS instead of directly connecting CMS power to the respective motor drivers. To disconnect power to these systems, a normally open relay is placed in series between the CMS voltage supply and the connection points for the drive and active suspension motors. For the relay to engage and provide power to the motors, the chassis-level E-stop module must provide a constant excitation voltage of 3.3 V to the PDS relay driving circuit (see Figure 11). The driving circuit is engineered with safety in mind, ensuring the relay rapidly disengages in E-stop conditions (3.3 V signal is not present). All power outputs from the PDS are fused using standard automotive AMT fuses, adding a layer of protection between the power pack, sensors, and actuators. The safe and regulated voltage supplied by the power pack enables the ECS to focus on the control and monitoring of the axle's actuators and sensors.

4.1.3. ECS

The ECS brings each axle to life, communicating with the vehicle's MCM and axle's PDS, monitoring feedback from the sensors, and applying the desired actuator outputs. At its core, the ECS has 7 main responsibilities:

1. Interface with the main motor drives to control torque and receive feedback.
2. Control the braking motors and provide torque feedback.

 doi:10.20944/preprints202603.1426.v1

3. Control the steering motors and provide position and torque feedback.
4. Interface with active suspension motor drivers and measure force feedback.
5. Measure the axle's suspension pose.
6. Receive actuator commands from and provide real-time feedback to the MCM.
7. Received power pack data from the axle's PDS.

The first four responsibilities are directly linked to the drive, brake, steering, and suspension-by-wire subsystems designed above. Each subsystem has a desired method of actuation and specified feedback to maximize vehicle control.

In drive-by-wire systems, the popular control input is drive motor torque, with feedback of the motor speed and applied torque. To facilitate torque control for the main drive motors, the SOLO UNO (SOLO Motor Controllers) - an off-the-shelf motor controller capable of motor torque or speed control with feedback - is implemented. The SOLO UNO boasts integrated analog and digital control modes, allowing the BLDC to be current (torque) or speed controlled based on an analog duty cycle and direction input, or digital UART or CAN communication. The device is capable of continuous motor monitoring via digital communication, streaming feedback data at 200 or 500Hz in monitoring mode. Two SOLO UNO V2 motor controllers are employed for each axle, each controlling one of the axle's drive motors. The ECS controls the motor torque using the analog control mode, where feedback is obtained using UART communication with the motor driver set to the 500 Hz continuous monitoring mode.

The brake-by-wire system (Section 3.3) and steer-by-wire (Section 3.5) systems employ a servo motor to apply the braking torque, and control the steering angle of each wheel. Servo motors are positionally controlled which is sufficient for the steer-by-wire system; however, the braking system must control torque. Therefore, the servos must be capable of implementing both position and torque feedback measurements. To obtain position feedback the servo's motor's internal wiring is accessed. A servo's internal control system uses a rotational potentiometer attached to its output shaft as feedback, with the potentiometer output representing a $0 - 3.3$ V linear scaling of the servo's rotation. Therefore, position feedback of the servo can be extracted from the potentiometer output, providing the ECS with an analog voltage based on the servo's current position. Torque feedback can be determined by measuring the current draw of the servo system (motor & controller), with the assumption that the internal servo controller has a constant current draw throughout operation. Placing a shunt resistor-based current sensor, with the corresponding differential and non-inverting amplifiers, between the servo's power supply (from the PDS) and the servo motor allows the total current drawn by the servo to be measured. One limitation is that the current sensor is only capable of detecting unidirectional current (torque). Servos commonly implement an internal proportional-derivative (PD) controller, where negative positional error leads to the application of negative torque. Therefore, the direction of the torque can be inferred based on the difference between the commanded and actual servo position. By identifying the servo's torque/current relationship, both the magnitude and direction of the servo's applied torque can be inferred as feedback. The implemented control system to achieve the desired braking torque and effective steering angle is presented later in section 4.2.

The future active suspension system described in Section 3.4.1 harnesses a 300 W direct current (DC) motor. DC motors are commonly driven by an H-bridge motor driver controlled by only a duty cycle signal and a direction pin. The active suspension system requires current (Torque/Force) to accurately control the desired suspension force. Current feedback can be obtained using a similar shunt resistor design used for the servo motor.

A core vehicle requirement is full-state feedback of the each of the vehicles DOFs (VSR2). The ECS is responsible for measuring the state of the driveline, steering, and suspension DOFs. The driveline feedback is achieved using the feedback from the SOLO UNO motor drives. However, to correctly measure the steering and suspension DOF the axle's suspension pose must be identified. The suspension pose is defined as the current position of each hardpoint of the double wishbone and steering systems displayed in Tables 1 and 2. To calculate the suspension pose, the position of the

 doi:10.20944/preprints202603.1426.v1

UCA or LCA, along with the steering motor position, must be known. In the suspension design, an absolute encoder is applied to the LCA to measure its rotation, where the steering servo motor is capable of providing the position feedback as described above. The identification of the suspension pose is explained in detail in Section 4.2 to follow.

The ECS remaining responsibilities are to enable inter-vehicle communication with the chassis's MCM and power packs PDS. The ECS facilitates communication using standard UART communication, exhibiting a master-slave relationship. Where the PDS only responds to an ECS command, and the ECS only responds to the MCM command. This method ensures that each message is properly received and processed, and ensures unnecessary data is not transmitted between devices. To directly achieve the required axle control outputs, low-level control systems are implemented within the axle's ECS.

4.2. Low-Level Control System & Kinematics Implementations

The main objective of the MARV platform from the lens of a control researcher is the ability to apply independent wheel drive torque (1), braking torque (2), effective steering angle (3), and active suspension vertical force (4), and achieve full state-feedback for each of the vehicle's subsystems (VSR1). To enable direct dictation of these control inputs, the ECS incorporates low-level control systems coupled with suspension kinematics for each subsystem, displayed in Figure 12. Analyzing the selected hardware, control inputs, and feedback requirements, only 1 control objective is directly realized with the selected hardware. Specifically, the SOLO UNO motor drivers enables the direct torque and monitoring, achieving objective 1 (Figure 12a). The remaining 3 objectives require low-level controllers operating on the ECS to realize the desired control objectives.

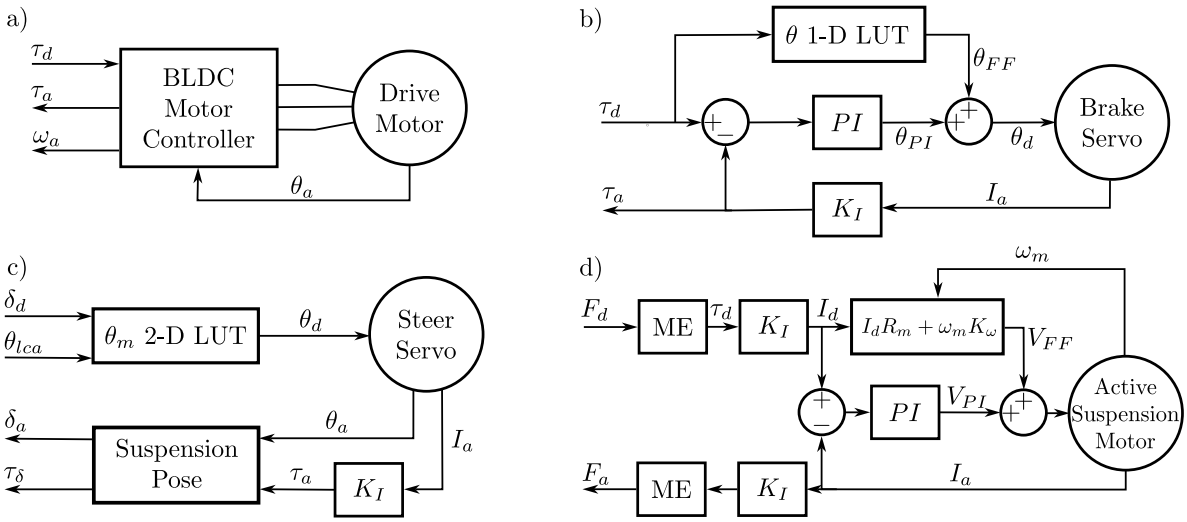

Figure 12. Axle level control systems: a) Driveline control with control input of desired motor torque (τ_d) and feedback of actual motor torque (τ_a) and speed (ω_a) , b) Braking control with control input of desired servo torque (τ_d) and feedback of actual servo torque (τ_a), c) Steering control with control input of desired effective steering angle (δ_d) and feedback of actual effective steering angle (δ_d) and steering torque (τ_δ), and d) Suspension control with control input of desired active suspension force (F_d) and feedback of actual suspension force (F_a).

4.2.1. Brake-by-Wire Control

The brake-by-wire system specifies a desired torque, where the servo motor employed is positionally controlled. To achieve the closed-loop torque control with a servo motor, a data-based feedforward-Proportional-Integral (FF-PI) controller is implemented (Figure 12b). The control method can be implemented due to the following assumption: The brake pads will not wear significantly throughout a single instance of vehicle operation. The assumption of negligible wear implies that the relationship between the servo commanded position and applied torque will remain constant. Therefore, on vehicle startup, the brake-by-wire systems can execute a calibration routine to generate a lookup table based on the servos' commanded position and measured current (torque). The lookup

 doi:10.20944/preprints202603.1426.v1

table is then directly referenced by the feedforward controller, setting the initial position of the servo based on the desired torque. The added PI controller augments the FF position by monitoring the error between the desired and measured motor torque. The FF portion is computed once per change in the control input signal, where the PI controller is implemented at 1 kHz.

4.2.2. Steering Control

To correctly apply an effective wheel steering angle, the required angular position of the steering motor must be calculated based on the current suspension pose. Figure 10 clearly depicts the large variation of steering motor angle required to maintain zero effective steering angle, directly compensating for bump-steer. The suspension pose is calculated in two steps: First, the positions of the lower and upper ball joints can be directly calculated in 3-dimensional space using the LCA encoder measurement, axis' of control arm rotation, and the geometries of the control arms and knuckle. Second, the position of the steering hardpoints can be analytically determined based on the position of the steering motor, identifying the rotation of the knuckle around the king-pin ($\hat{k}$) axis. As described in Section 3.5, the effective steering angle is defined by the spindle unit vector, dependent on the applied steering rotation about the kingpin axis (δ_k). The result is a spindle vector that can only be defined in forward calculations, requiring a fully defined suspension pose.

Therefore, similar to the BBW feedforward controller, the SBW controller implements a data-based feedforward control, relying on a 2-dimensional lookup table to identify the required steering motor angle (θ_m) to achieve the desired effective steering angle (δ_{eff}) based on the current LCA angle (θ_{LCA}). On startup, the suspension hardpoints are pre-calculated for the specified ranges of θ_{LCA} and θ_m and stored in a lookup table (Figure 12c). While the method discretizes the continuous forward calculation, the effects of discretization are minimized as the look-up table size increases. In this case, the 2-Dimensional lookup table was of size 128×128 for $\theta_{LCA} \in [0.2531, -0.4693]$ rad and $\theta_m \in [1.0472, -1.0472]$ rad, resulting in an angular resolution of $5.6e-3$ and $1.6e-2$ rad, respectively. The proposed control system operates at a frequency of 100 Hz, identifying the values of θ_m in the lookup tables based on the measured θ_{LCA} and desired δ_{eff}.

4.2.3. Active Suspension Control

The final low-level control system targets torque/force control of the future active suspension system. A H-bridge motor driver allows the voltage to the DC motor to be directly controlled and the current monitored by the shunt-based current sensor. The proposed controller is a model-based FF-PI controller, where the model-based FF component incorporates the motor's speed, torque and speed constants, and lumped electrical properties to model the required input voltage to the motor to generate the desired motor current (torque) (Figure 12d). The added PI controller augments the model-based FF controller to account for system uncertainties and ensure the desired setpoint is achieved. The controller is proposed to operate at 2 kHz to accommodate the high-speed current transients in DC motors.

The presented ECS embedded device and corresponding low-level control system creates the capability to realize the desired control inputs and capture the desired feedback for advanced XBW vehicle control algorithms implemented on the chassis level of the vehicle's architecture.

4.3. Chassis Level

The chassis level of the system architecture is designed to coordinate the vehicles axles (VSR1), provide remote monitoring and feedback (VSR5) and enable to implemation of advanved vehicle control systems (VSR6). This capability is realized by the MCM, while the independent E-stop module provide the capability to stop the vehicle in case of an emergency.

4.3.1. MCM

The vehicle's MCM is responsible for interfacing with each axle and the operator, while logging vehicle data and executing complex vehicle control algorithms in real-time. The axle-level embedded

 doi:10.20944/preprints202603.1426.v1

systems are designed to minimize the computational load on the MCM by ensuring its only interaction with the vehicle itself is with the ECS and a single chassis IMU and GNSS device. The combined IMU and GNSS device measures the chassis' 6-DOF body translation and rotation, the only DOFs not measured by each axle's ECS. The design allows for a computer-on-module to be implemented, in this case a Raspberry Pi 5 (8 GB Ram, A76 2.4 GHz processor). For the presented two-axle vehicle, the MCM communicates with the front and rear axle's ECS with UART and powers and communicates with the IMU and GNSS via USB. A multi-threaded C++ API was developed for the vehicle, instantiating individual threads to communicate with each ECS, the IMU and GNSS device, data logging, and to service an external wireless controller for manual vehicle control validation. The API allows a control system designer to directly apply the vehicle control inputs of: Drive motor torque, braking torque, effective wheel steering angle, and future active suspension force for each wheel. The API provides full-state feedback values of: Standard IMU and GNSS reading, measured drive motor torque, wheel speeds, effective steering angle, rotation and rotational velocity of the knuckle around the kingpin axis ($\hat{k}$), applied steering torque to the kingpin axis, applied active suspension force, suspension displacement and velocity, and an estimate of tire vertical force and effective radius. In addition, the API also provides the battery pack voltage and average current draw, main motor controller temperatures, and the status' of the ECS, PDS, and CMS embedded systems. The API can facilitate a control loop frequency of up to 100 Hz, limited by ECS communication bandwidth. Although the MCM control loop frequency is much lower than the low-level control loops, it surpasses the requirements for larger high-level control algorithms, such as model predictive control, which have lower control step times due to their high computational load.

4.3.2. E-Stop

An important aspect in both research devices and industrial machinery is the capability to directly de-energize a system and ensure safe termination of its operation during an emergency condition. In the case of an emergency, an operator or bystander presses an E-stop button, which physically disconnects power to the main power relay for actuators and applies mechanical brakes according to the country of operation's safety standards organization. In remotely operated vehicles, a person is unable to press a physically wired E-stop to disconnect the power from the system. Therefore, a wireless E-stop system was designed to create a wireless link between the operator's E-stop controller and the vehicle's E-stop module.

To create the wireless link, two dedicated microcontrollers are assigned for the emergency stop controller (operator) and the emergency stop module (chassis). The wireless link is facilitated by a LoRa (915 MHz) transmitter and receiver module with a transmission gain of 20 dBm and transmit and receiver antenna gains of 5 dBi. To establish the wireless link, the transmitter (operator) continuously transmits a specified message. The receiver, within the vehicle's emergency stop module, receives and parses the transmitted message. If the received message matches the expected message for a specified number of successive messages, the vehicle's E-stop module enables the PDS relay (see Section 4.1.2), allowing power to be supplied to the main drive and active suspension motor controllers. Once active, the vehicle's E-stop module must continue to receive the correct message from the transmitter at least once per 300 milliseconds. Failure to receive a message results in the PDS relay disabling, and disconnecting propulsive power from the vehicle. The power supplied to the E-stop controller (transmitter) is directly fed through an industrial grade E-stop button. With the proposed design, the vehicle will transition into an E-stop condition under the following two conditions: 1) The E-stop button is pressed, directly de-energizing the E-stop LoRa transmitter, or 2) The vehicle operates out of range of the E-stop transmitter, leading to incomplete or no messages received by the vehicle.

The mechanical, electrical, embedded, and low-level control systems presented outline the multi-domain design aspects required to realize the full MARV XBW test platform. The process to converge upon the presented design was iterated over many configurations, eventually resulting in the operational experimental vehicle platform presenting in this work.

 doi:10.20944/preprints202603.1426.v1

5. Complete Vehicle Assembly

The culmination of the multi-domain design project led to the design, manufacture, and assembly of the MARV platform depicted in Figure 13. The outcome is a fully SDV with drive, steer, brake, and future suspension-by-wire capabilities. To apply and validate advanced XBW control systems, the constructed vehicle, along with its mechanical and electrical subsystems, must be calibrated through system identification.

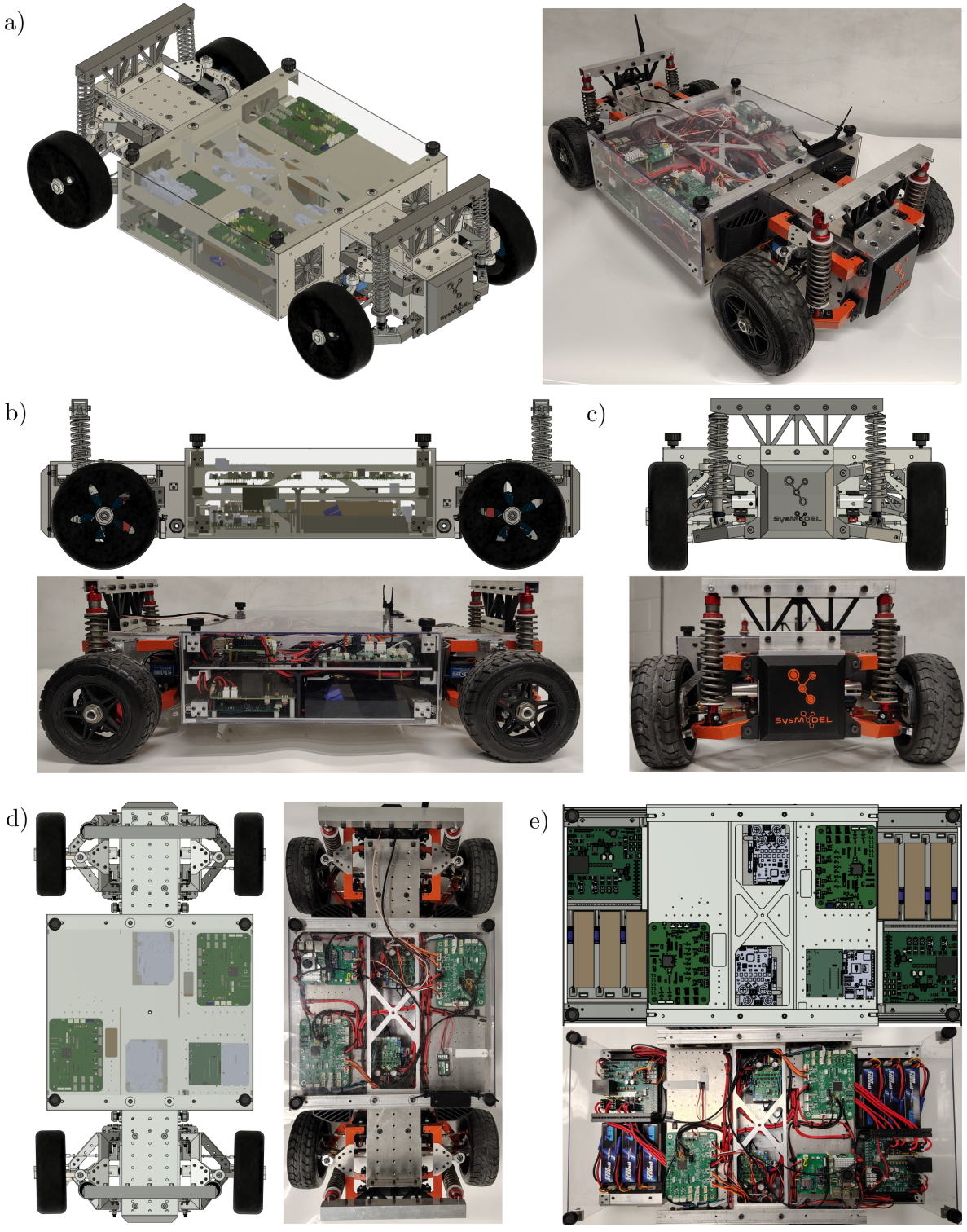

Figure 13. Developed MARV platform outlining the a) isometric, b) side, c) front, and d) top view of the CAD model and manufactured two axle vehicle. e) Displays the chassis's body components and the wiring required to connect the mechanical, electrical, and embedded subsystems.

 doi:10.20944/preprints202603.1426.v1

6. System Identification

The presented XBW vehicle is complex and requires significant static and dynamic system identification for the mechanical, electrical, and software systems. Therefore, due to the large scope of system identification, only preliminary system identification is presented to enable testing and validation of the VSRs, specifically the performance requirements in VSR3. The system identification is separated into mechanical, electrical, and software subsections.

6.1. Mechanical

The vehicle's mechanical system identification is limited to determining the vehicle's assembled mass, including the batteries, wiring, and circuit boards. The vehicle was measured using a laboratory scale with an accuracy of 0.01 kg. The assembled vehicle mass is measured as 28.95 kg, below the targetted vehicle mass of 35 kg. In addition, the key mechanical components and mounting locations were measured to ensure they conform to the specified design tolerances.

6.2. Electrical

Within the vehicle's electrical system, each ECS electrical feedback mechanism was characterized. First, the current sensors for the brake and steering servo motors are characterized using an electronic load. The load current and measured sensor output are compared and fit to a linear equation. The servo motor position feedback was characterized using an absolute encoder, comparing the analog position output from the servo with the encoder position, resulting in a linear relationship. Both the servos' position and encoders feedback on the vehicle require global position calibration. For the servos, calibration is completed by deactivating the servo and placing the output shaft in a known position, and recording the position offset. The encoders on the LCA are calibrated similarly, rotating the LCA to a known position and recording the offset.

6.3. Software

The ECS software systems were tested to ensure the desired control loop sample times were achieved. Using a logic analyzer with extra breakout pins on the ECS, the execution time and frequency for key tasks were monitored. The results showed that the ECS is fully capable of executing its tasks described in sections 4.1.3 and 4.2, well within its sample time, boasting only a 23.2% processor utilization. The utilization can be separated into communication (1.8%), scheduled task executions (15.1%), servo position and current feedback (3.27%), and scheduler services and communication timeout watchdogs (3.17%). A key portion to highlight is the computation time attributed to calculating the axles' suspension pose within the scheduled task executions on the ECS. The suspension calculations alone attribute to 8.5% of the total processor utilization with the help of lookup tables. Using this method, the processor requires only 880 microseconds to calculate the full suspension pose for both left and right suspensions, including all 3D point locations and key suspension characteristics such as mechanical trail, scrub, radius, effective steering angle, and camber angle.

7. Experimental Results

An experimental test campaign was performed, focused on ensuring vehicle dynamic capabilities are achieved (VSR3). In total, three experiments were performed: 1) A front wheel drive acceleration test (VSR3-a), 2) A rear wheel braking stopping distance test (VSR3-c), and 3) a turning radius test (VSR3-d). The front wheel driveline and rear wheel braking configuration was intentionally selected due to the presence of longitudinal load transfer during acceleration and braking, placing the vehicle in its worst case configuration for the respective experiments. The top speed requirement in VSR3-b was not tested due to the testing environment's spatial limits and safety considerations.

Experiments 1 and 2 are completed in the same test. First, the vehicle is commanded to accelerate at its maximum possible rate until a speed of 5.26 m/s, completing experiment 1. Second, the vehicle enters a drifting phase for > 1 second to create separation between the two experiments. Third,

 doi:10.20944/preprints202603.1426.v1

the braking test is conducted using the brake-by-wire system to lock the rear wheels, completing experiment 2 when the vehicle successfully stops.

To conduct the test, a simple vehicle controller is implemented on the vehicle's MCM at 100 Hz, handling the drive motor torque, speed observation, and elapsed time measurements. The vehicle's data logger tracks the vehicle states at a frequency of 50 Hz. Figure14, displays the results of experiment 1 and 2. Experiment 1 led to a $0 \rightarrow 5.26$ m/s time of 3.9 seconds, within the 5.2 second requirement presented in VSR3-a. While the top speed requirement was not tested on the vehicle, the top speed of each of the vehicle's four drivelines' maximum speed was tested independently. The lowest and highest peak driveline speeds of 194 and 198 rad/s , leading to potential vehicle speeds of 16.49 m/s and 16.83 m/s, respectively. Based on the preliminary results, it is foreseen that the vehicle will fall short of the desired top speed of 16.67 m/s due to tire rolling resistance and aerodynamic drag. Experiment 2 resulted in a stopping distance of 4.54 m from an initial speed of 4.68 m/s, below the specified speed of 5.26 m/s. Analyzing the deceleration of the vehicle in Figure 14, the braking tests exhibit a linear trend. Thus, using the same rate of deceleration from the experiment, the adjusted stopping distance from 5.26 m/s is 5.61 m, within the VSR3-c requirement of 7.69 m.

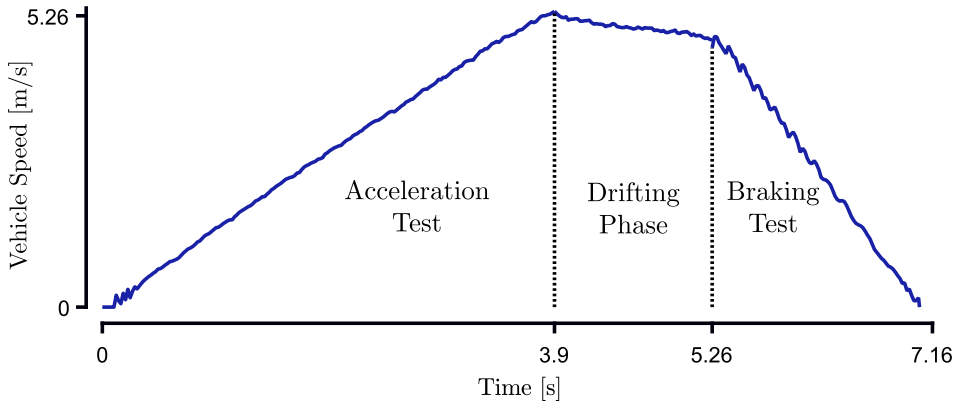

Figure 14. Experiment 1 and 2 results, displaying the vehicle's velocity during the combined acceleration and braking test.

The final experiment studies the vehicle's steer-by-wire capabilities. The vehicle's suspension was loaded in the 1G conditions, and the maximum effective steering angle for the front and rear wheels was measured using the steering system feedback measurements. The result is a maximum steering angle of 0.5 rad and 0.45 rad for the front and rear axles, respectively. The difference in steering angles is due to the change in LCA design to facilitate the positive mechanical trail, leading to earlier spatial restrictions between the tire and LCA for the rear suspension system. Using the Ackerman steering principle with the maximum front and rear steering angles, the front wheel, rear wheel, and all wheel turning radii are 1.45 m, 1.60 m, and 0.84 m, respectively. Each steering configuration is within the desired 2.30 m steering radius presented in VSR3-e.

8. Conclusion & Future Work

In conclusion, this work presented the systematic design of a 1:5 scale multi-actuated research vehicle (MARV) platform. A systematic design process is applied, highlighting the key vehicle specifications and subsequent subsystem engineering requirements. A high-level overview of the platform's mechanical, electrical, embedded, and software systems was presented, followed by the identification of critical systems and experimental validation of the assembled vehicle. The produced vehicle platform is capable of achieving the outlined vehicle specification, speaking to the efficacy of a systematic and comprehensive design process.

The resultant MARV platform opens the door for scaled testing of over-actuated vehicle combinations not seen before in a research arena. The SDV allows researchers to compare and contrast different actuator configurations and control architectures on a palatable test platform. Specifically, MARV

 doi:10.20944/preprints202603.1426.v1

enables emulation of traditional vehicle driveline and steering configurations (e.g. front wheel drive with linked steering), facilitating the comparison of any vehicle actuator configuration. Furthermore, the independent wheel steer capability enables emulation of various vehicle wheel bases and track widths, extending the vehicle's versatility. Overall, the MARV platform creates a vehicle-agnostic framework to test and validate unique actuator combinations and advanced control algorithms.

Future work related to the MARV platform will be focused on three main areas: 1) The integration of active suspension mechanisms as initially described in section 3.4.1. 2) The development of a digital twin of the MARV platform using the Project Chrono Vehicle library [18], creating a sandbox environment to foster the development and preliminary testing of advanced control algorithms with multi-actuated vehicles. 3) Experimental validation of multi-actuated control algorithms using the MARV platform, capturing the improvements in safety and performance enabled by vehicle over-actuation.

Funding: This platform development was supported by ResearchNB Lab-2-Market (RNB-L2M-0000000141)

Acknowledgments: The authors would like to acknowledge the contributions of the following individuals to both the early and current development of the MARV platform: Dr. Meaghan Charest-Finn, Salman Khalid, Caleob Maher-Watson, Anh Albert Nguyen, Eke Kalu, Owen Fletcher, Quynh Nguyen, Liam Arsenault, Dustin Jennings, Andrew MacDonald, William Sanford, Mikael Langlois, Payton Cross, Spierings Verhoeven, Evan LeGresley, Ethel Padilla, Alejandra Pena, Govind Ramesh, Tyler Matheson, Samuel Bain, and Robert McGibbon.

References

1. FAVRE, C. Fly-by-wire for commercial aircraft: the Airbus experience. *International Journal of Control* **1994**, *59*, 139–157. https://doi.org/10.1080/00207179408923072.
2. Bretz, E. By-wire cars turn the corner. *IEEE Spectrum* **2001**, *38*, 68–73. https://doi.org/10.1109/6.915192.
3. Li, D.; Tan, C.; Ge, W.; Cui, J.; Gu, C.; Chi, X. Review of Brake-by-Wire System and Control Technology. *Actuators* **2022**, *11*, 80. https://doi.org/10.3390/act11030080.
4. Hua, X.; Zeng, J.; Li, H.; Huang, J.; Luo, M.; Feng, X.; Xiong, H.; Wu, W. A Review of Automobile Brake-by-Wire Control Technology. *Processes* **2023**, *11*, 994. https://doi.org/10.3390/pr11040994.
5. Huang, C.; Naghdy, F.; Du, H.; Huang, H. Fault tolerant steer-by-wire systems: An overview. *Annual Reviews in Control* **2019**, *47*, 98–111. https://doi.org/10.1016/j.arcontrol.2019.04.001.
6. Mortazavizadeh, S.A.; Ghaderi, A.; Ebrahimi, M.; Hajian, M. Recent Developments in the Vehicle Steer-by-Wire System. *IEEE Transactions on Transportation Electrification* **2020**, pp. 1226–1235. https://doi.org/10.1109/TTE.2020.3004694.
7. Zhang, L.; Zhang, Z.; Wang, Z.; Deng, J.; Dorrell, D.G. Chassis Coordinated Control for Full X-by-Wire Vehicles-A Review. *Chinese Journal of Mechanical Engineering* **2021**, *34*, 42. https://doi.org/10.1186/s10033-021-00555-6.
8. Funke, J.; Brown, M.; Erlien, S.M.; Gerdes, J.C. Collision Avoidance and Stabilization for Autonomous Vehicles in Emergency Scenarios. *IEEE Transactions on Control Systems Technology* **2017**, *25*, 1204–1216. https://doi.org/10.1109/TCST.2016.2599783.
9. Dallas, J.; Talbot, J.; Suminaka, M.; Thompson, M.; Lew, T.; Orosz, G.; Subosits, J. Control Barrier Functions for Shared Control and Vehicle Safety. In Proceedings of the 2025 American Control Conference (ACC), 2025, pp. 4203–4210. arXiv:2503.19994 [eess], https://doi.org/10.23919/ACC63710.2025.11107628.
10. Wallmark, O.; Nybacka, M.; Malmquist, D.; Burman, M.; Wennhage, P.; Georen, P. Design and Implementation of an Experimental Research and Concept Demonstration Vehicle. In Proceedings of the 2014 IEEE Vehicle Power and Propulsion Conference (VPPC), 2014, pp. 1–6. ISSN: 1938-8756, https://doi.org/10.1109/VPPC.2014.7007042.
11. Brembeck, J.; Ho, L.M.; Schaub, A.; Satzger, C.; Tobolar, J.; Bals, J.; Hirzinger, G. ROMO - The Robotic Electric Vehicle. In Proceedings of the 22nd IAVSD International Symposium on Dynamics of Vehicle on Roads and Tracks, Manchester, Großbritannien, 2011.
12. O'Kelly, M.; Zheng, H.; Karthik, D.; Mangharam, R. F1TENTH: An Open-source Evaluation Environment for Continuous Control and Reinforcement Learning. In Proceedings of the Proceedings of the NeurIPS 2019 Competition and Demonstration Track. PMLR, 2020, pp. 77–89. ISSN: 2640-3498.
13. Gonzales, J.M. Planning and Control of Drift Maneuvers with the Berkeley Autonomous Race Car. Ph.D., University of California, Berkeley, 2018. ISBN: 9780438325753.

 doi:10.20944/preprints202603.1426.v1

14. Goldfain, B.; Drews, P.; You, C.; Barulic, M.; Velev, O.; Tsiotras, P.; Rehg, J.M. AutoRally An open platform for aggressive autonomous driving, 2018. https://doi.org/10.48550/arXiv.1806.00678.
15. Samak, C.V.; Samak, T.V.; Velni, J.M.; Krovi, V.N. Nigel – Mechatronic Design and Robust Sim2Real Control of an Over-Actuated Autonomous Vehicle, 2024. https://doi.org/10.48550/arXiv.2401.11542.
16. Calvo, J.; Diaz, V.; San Román, J. Establishing inspection criteria to verify the dynamic behaviour of the vehicle suspension system by a platform vibrating test bench. *International journal of vehicle design* **2005**, *38*, 290–306.
17. DeBoer, B.; Kimball, J.B.; Bubbar, K. Design, Control, and Validation of a Brake-by-Wire Actuator for Scaled Electric Vehicles. *IEEE Robotics and Automation Letters* **2024**, *9*, 4695–4701.
18. Serban, R.; Taylor, M.; Negrut, D.; Tasora, A. Chrono:: Vehicle: template-based ground vehicle modelling and simulation. *International Journal of Vehicle Performance* **2019**, *5*, 18–39.
19. Gillespie, T. *Fundamentals of vehicle dynamics*; SAE international, 2021.
20. ISO 8608: Mechanical vibration — Road surface profiles — Reporting of measured data, 2016.
21. Stauder, K.; Ma, R. 10s Battery Pack Monitoring, Balancing, and Comprehensive Protection, 50A Discharge Reference Design. Design Guide TIDA-00449, Texas Instruments, 2019.